Ossabaw Pigs With a PCSK9 Gain-of-Function Mutation Develop Accelerated Coronary Atherosclerotic Lesions: A Novel Model for Preclinical Studies

Fang Yuan, MD;* Liang Guo, PhD;* Kyoung-Ha Park, MD, PhD;* John R. Woollard, MSc; Kwon Taek-Geun, MD, PhD; Kai Jiang, PhD; Tamene Melkamu, DVM, PhD; Bin Zang, BS; Samantha L. Smith, BS; Scott C. Fahrenkrug, PhD; Frank D. Kolodgie, PhD; Amir Lerman, MD; Renu Virmani, MD; Lilach O. Lerman, MD, PhD;† Daniel F. Carlson, PhD†

Background—Ossabaw pigs are unique miniature swine with genetic predisposition to develop metabolic syndrome and coronary atherosclerosis after extended periods receiving atherogenic diets. We have hypothesized that transgenic Ossabaw swine expressing chimp *PCSK9* (proprotein convertase subtilisin-like/kexin type 9) containing the D374Y gain of function would develop familial hypercholesterolemia and coronary artery plaques more rapidly than Landrace swine with the same transgene.

Methods and Results—Ossabaw and Landrace *PCSK9* gain-of-function founders were generated by *Sleeping Beauty* transposition and cloning. Histopathologic findings in the Ossabaw founder animal showed more advanced plaques and higher stenosis than in the Landrace founder, underscoring the Ossabaw genetic predisposition to atherosclerosis. We chose to further characterize the Ossabaw *PCSK9* gain-of-function animals receiving standard or atherogenic diets in a 6-month longitudinal study using computed tomography, magnetic resonance (MR) imaging, intravascular ultrasound, and optical coherence tomography, followed by pathological analysis of atherosclerosis focused on the coronary arteries. The Ossabaw model was consistently hypercholesterolemic, with or without dietary challenge, and by 6 months had consistent and diffuse fibrofatty or fibroatheromatous plaques with necrosis, overlying fibrous caps, and calcification in up to 10% of coronary plaques.

Conclusions—The Ossabaw *PCSK9* gain-of-function model provides consistent and robust disease development in a time frame that is practical for use in preclinical therapeutic evaluation to drive innovation. Although no animal model perfectly mimics the human condition, this genetic large-animal model is a novel tool for testing therapeutic interventions in the context of developing and advanced coronary artery disease. (*J Am Heart Assoc.* 2018;7:e006207. DOI: 10.1161/JAHA.117.006207.)

Key Words: atherosclerosis • coronary artery disease • PCSK9 • pig

The healthy domestic swine model is currently relied on for preclinical safety and performance testing of therapeutic interventions intended to treat cardiovascular diseases. Because of the lack of coronary pathological features, a swine model that replicates human coronary artery disease has been pursued for decades.[1,2]

Swine with naturally occurring low-density lipoprotein receptor (*LDLR*) and *APOB* mutations are related to a frequently used large-animal model of cardiovascular disease, the Rapacz model. Experience with this model has shown that attaining a consistent effect on lesion development with a traditional breeding and selection approach is challenging.[3] More recently,

---

Clinical Perspective

What Is New?

- An Ossabaw miniature swine model of hypercholesterolemia and atherosclerosis expresses a gain-of-function PCSK9 (proprotein convertase subtilisin-like/kexin type 9) protein with high homology to humans.

What Are the Clinical Implications?

- This is a preclinical model for testing drugs to reduce cholesterol or atherosclerotic conditions before entering the clinic.
- This is a preclinical model for testing safety or efficacy of devices for coronary or peripheral atherosclerosis.
- This is a model to test novel imaging techniques or biomarkers of atherosclerosis.

---

an *LDLR* gene knockout model has been reported in Yucatan and conventional swine.[4,5] Homozygous animals had pronounced dyslipidemia, and after 4 to 6 months consuming a modified diet, some advanced lesion development was observed in the abdominal aorta and coronary arteries of Yucatan and conventional swine, respectively. Although this represents an improvement in atherosclerosis modeling, models compatible with emerging cholesterol-lowering therapies targeting *PCSK9* (proprotein convertase subtilisin-like/kexin type 9)[6,7] would be useful. In addition, although domestic swine have excellent fecundity (litters of 10+ versus 4–6 for minipigs), they rapidly outgrow practical research approaches, such as the use of clinical tools.

PCSK9, a major regulator of LDL receptor recycling and LDL fate in pigs and humans, is a more recently appreciated factor in atherosclerosis and cardiovascular disease.[8–10] Rare *PCSK9* gain-of-function (GOF) mutations are linked to familial hypercholesterolemia in humans.[11] One particular GOF mutation, which substitutes an aspartic acid for tyrosine at amino acid 374 (D374Y), causes a particularly severe disease phenotype in heterozygous individuals.[12–15] Hence, the *PCSK9-D374Y* mutation makes an excellent target from the standpoint of modeling familial hypercholesterolemia in swine because of strong, fully penetrant, and dominant effects on LDL. Indeed, *PCSK9-D374Y* transgenic Yucatan swine have been studied and show significant elevations in total and LDL cholesterol (LDLc), but not triglycerides,[16] and lesions observed in the coronary arteries were predominantly an early-stage event after 11 to 12 months receiving high-fat and high–cholesterol (HFHC) diet.

In contrast to Yucatan and conventional swine breeds, Ossabaw swine have a large capacity for fat deposition and vascular disease, and they have higher levels of fasting triglycerides and nonfasting insulin compared with conventional swine.[17–20] Similar to other swine, Ossabaw fed an HFHC diet develop dyslipidemia, but distinctively develop diffuse coronary lesions subsequent to stent placement.[21] Multiple studies have demonstrated insulin resistance and metabolic syndrome in the Ossabaw breed, which significantly increase the comorbidity risk of diabetes mellitus and cardiovascular disease in humans, suggesting that it presents a valuable genetic background for swine model development.[22–28] Therefore, we hypothesized that incorporation of *PCSK9-D374Y* in this susceptible breed will produce a robust model with reduced latency and improved consistency for atherosclerotic lesion development.

Methods

The study was approved by the Institutional Animal Care and Use Committee. The data, analytic methods, and study materials are available by request to other researchers for purposes of reproducing the results or replicating the procedure.

Vector Construction

The PCSK9 coding sequence was derived from the *Pan troglodyte* coding sequence (GenBank: EF692497.1). The coding sequence is positioned downstream from a liver-specific fusion promoter, consisting of albumin enhancer coupled with the human α-1 antitrypsin promoter. The promoter construct and PCSK9-D374Y coding sequence were produced through a commercially available solid state gene synthesis service, and the coding sequence was codon optimized for expression in swine (Epoch Life Sciences). The commercially supplied pBSK-E-AT-PCSK9 D374Y plasmid was digested with SpeI and BglII restriction endonucleases and cloned into the pKT2C-EGFP[29] transposon plasmid digested with the same enzymes to produce pKT2-E/AT-PCSK9-D374Y. The pKT2/PGK-PuroDtk and pKC-SB11 vectors were described previously.[29]

Production of Cloned Minipigs With PCSK9 GOF Mutant

Pig fibroblasts were isolated from 43-day-old fetuses of Ossabaw minipig (Swine Resource, Indiana University, Bloomington, IN) or 43-day-old Landrace fetuses. The tissue was dissociated using a collagenase/DNaseI treatment and mechanical disruption, and tissue was cultured in DMEM enriched with 10% fetal bovine serum and antibiotic/antimycotic solution (Invitrogen, Carlsbad, CA). For transfection, passage 0 fibroblasts were thawed and plated in DMEM high-glucose media enriched with 10% fetal bovine serum,

2 mmol/L L-glutamine, and penicillin/streptomycin (Invitrogen, Carlsbad, CA) and grown at 38C°, 5% CO_2. A 5:1:3 cocktail of gene-of-interest transposon (10 μg; pKT2-E/AT-PCSK9-D374Y):selection marker transposon (pKT2/PGK-PuroDtk):pKC-SB11 was introduced into 1.0×10^6 PFF cells by nucleofection using the Basic Fibroblast Nucleofection kit (Lonza). After a 48-hour recovery, a portion of the transfected cells was plated on 2 96-well plates at densities of 5 and 50 cells/well. To aid in plating efficiency, nontransfected cells were included to result in a final density of 1000 cells/well before selection. The remaining cells were plated in 100-mm plates at densities of 20 000 and 100 000 cells/plate and selected in 1.2 μg/mL of puromycin for 10 to 14 days. Because of extremely high coretention of the gene-of-interest by this method,[30] pools of puromycin-resistant cells from the 100 000 cells/plate condition were used directly for cloning of founders. All cloned reconstructed embryos were produced under license of Chromatin Transfer technology[31] from Hematech to Cooperative Resources International Center for Biotechnology (Verona, WI). Oocyte collection, maturation, and micromanipulation and embryo transfer were performed following established standard operating procedures. Founder animals 1513 were cloned from the pooled puromycin-resistant cells. All animals enrolled in the in vivo study were produced by cloning of adult derived fibroblasts from 1513.

Genome Sequencing and Insertion Mapping of 1513

Genomic DNA from Ossabaw 1513 was sequenced to a ×30 coverage using Illumina paired-end sequencing. Insertions sites were identified by comparison to the reference genome. First, reads that overlap with the inserted sequence were extracted, the flanking region was identified, and the scaffold around the PCSK9 insert was reconstructed by iteratively expanding the overhanging sequence. Second, we mapped the whole genome sequence reads to the reference pig genome. Soft clipped reads (reads that are partially mapped) are then extracted and aligned to the insert sequence. By combining the results from these steps, we reconstructed all 3 flanking sequences of the PCSK9 inserts. The entire workflow is implemented using a customized python script integrating bowtie2, fastq-extract, samtools, and mosaic.[32–34] The coordinates of the flanking sequences were mapped using BLAST against the Sscrofa11.1 reference genome from National Center for Biotechnology Information.

Study Groups and Experimental Design

Cloned *PCSK9* GOF Ossabaw swine (3 months old; Recombinetics, Inc, St Paul, MN) were fed either a standard chow (PCSK9 GOF, 13% protein, 2% fat, 6% fiber; Purina Animal Nutrition LCC, MN) or an atherogenic diet (PCSK9 GOF atherogenic, 23% fat, 15.9% sucrose, 2% cholesterol) for 6 months (n=7 each). Wild-type Ossabaw male clones (3 months old), cloned by the methods previously described from a separately derived line of male fetal fibroblasts, fed with standard chow served as controls (n=7).

Before initiation of diet, telemetry transducers (DSI, St Paul, MN) were implanted in the femoral arteries of all pigs. Blood pressure was subsequently measured and averaged for 3 days before each in vivo study. At 3 and 6 months after initiation of diet, blood oxygen level–dependent MR imaging, multidetector computed tomography (MDCT), and intravascular imaging studies were performed to assess cardiac oxygenation, function, and the coronary arteries, respectively. Myocardial blood oxygen level–dependent MR imaging is a non–contrast-enhanced noninvasive approach to assess myocardial oxygenation by the signal generated by endogenous deoxyhemoglobin in the blood.[35] MDCT affords evaluation of cardiac structure and function.[36] In addition, we used contrast-enhanced CT angiography (CTA),[36] intravascular ultrasound (IVUS), and optical coherence tomography (OCT)[37] for a comprehensive in vivo assessment of atherosclerotic lesion development and progression. Under anesthesia (IV 5 mg/kg telazol plus 2 mg/kg xylazine), in intubated and mechanically ventilated pigs, catheters were placed in the carotid arteries, blood samples were drawn for lipid panel and PCSK9 protein quantification, and imaging studies were then performed. At 1 week after completing all in vivo studies, pigs were euthanized with sodium pentobarbital (100 mg/kg IV Fatal Plus; Vortech Pharmaceuticals, Dearborn, MI). The heart was immediately removed and prepared for micro-CT studies or perfused and preserved in formalin for histopathological studies. Liver samples were collected to assess PCSK9 and LDL receptor by Western blot.

Systemic Measurements

Systemic plasma total cholesterol (TC), triglycerides, LDLc, and high-density lipoprotein cholesterol levels were measured by standard procedures. Secreted PCSK9 protein concentration was determined in plasma (diluted at 1:800) using human PCSK9 Quantikine ELISA kit (DPC 900; R&D Systems, Minneapolis, MN), following manufacturer's protocol. Nuclear MR lipid concentrations and size measurements were performed by the Immunochemical Core Lab (Mayo Clinic, Rochester, MN) with the standard human protocol. Heart rate was recorded using an intra-arterial catheter during the imaging session. Mean blood pressure was assessed as the average area under the telemetry recorded pressure curve. Rate-pressure product, an index of cardiac oxygen consumption, was calculated as the product of resting heart rate and systolic blood pressure.

In Vivo Studies

Blood oxygen level–dependent MR imaging

Myocardial blood oxygen level–dependent MR imaging scans were performed on a 3.0-T scanner (Signa EXCITE; GE Healthcare, Waukesha, WI) to assess myocardial oxygenation. Short-axis images were acquired using an ECG-gated spoiled gradient echo sequence during suspended respiration. The imaging parameters were as follows: repetition time, 1 R-R interval; echo time, 2.2 to 11.6 milliseconds; number of echoes, 8; matrix size, 128×128; field of view, 35×35 cm^2; slice thickness, 5 mm; and flip angle, 30°. Myocardial R2* was quantified pixel-wise by an exponential fitting of the MR signal intensity versus echo times using in-house developed Matlab software (Matlab 7.10; The MathWorks, Natick, MA), as described previously.[38,39] The region of interest was manually traced on the T2*-weighted images with an echo time of 7.6 milliseconds.

Multidetector CT

To evaluate cardiac function and microvascular function, MDCT (SomatomFlash-128; Siemens Medical Solution, Forchheim, Germany) images were acquired and analyzed using Analyze (Biomedical Imaging Resource, Mayo Clinic), as shown previously.[38,39] A 50-second flow scan followed a bolus injection of the contrast medium iopamidol (0.33 mL/kg over 2 seconds) into the right atrium to evaluate myocardial perfusion in the lateral left ventricular (LV) wall.[40] Subsequently, the entire LV was scanned 20 times at multilevels throughout the cardiac cycle for measurement of indexes of LV systolic (cardiac output and LV ejection fraction) and diastolic (E/A ratio) function, as well as LV muscle mass. Cardiac volume and pericardial fat (density between −190 and −30 Hounsfield units)[41] were then traced manually at each cross-section, as shown.[38–40] Pericardial fat was assessed as adipose tissue enclosed by the visceral pericardium, expressed as a fraction of cardiac volume.

CT angiography

CTA images were reconstructed from the cardiac volume scan to assess coronary artery diameters, lesions, and luminal narrowing. Aquarius iNtuition viewer (4.4.11; TeraRecon, Inc) was used for semiautomatic quantitative analysis by an experienced examiner.[42,43] Briefly, a fast vessel-tracking algorithm defined the center line of the coronary artery, and straightened multiple planar reformatted volume images were reconstructed. Multiple planar reformatted volume-deprived longitudinal contours and concomitant transverse contours, based on an initial approximation of the lumen border locations of longitudinal contours, were established by the algorithm, with manual editing and adjustment if indicated.

For identified lesions, reference diameter, minimal lumen diameter, diameter stenosis (% DS), and lesions length were obtained. The diameters of each coronary vessel at its ostium, middle, and distal segments were measured using the 17 coronary segments model, according to the American Heart Association classification.[44] Luminal DS was calculated as the ratio between the smallest luminal diameter and the average reference diameter proximal and distal to the lesion.

IVUS and OCT

To assess vascular wall pathological features, IVUS and OCT studies were performed after the MDCT scan, as described previously.[45,46] In brief, after intracoronary administration of 100 to 200 µg nitroglycerin, a 0.014-inch guide wire was advanced into the distal left anterior descending artery (LAD). A 20-MHz IVUS catheter (Volcano; Eagle Eye Gold, Rancho Cordova, CA) was advanced into the middle to distal LAD, and automatic pullback was done (0.5 mm/s). IVUS images were recorded on a DVD. Offline volumetric reconstruction and virtual histological analyses were performed by an independent experienced examiner "blinded" in 20-mm segment of the proximal LAD using the Volcano Image Analysis software V3.1. Quantitative volumetric analysis included the average vessel volume (mm^3) (average vessel area×20 mm), average lumen volume (mm^3) (average lumen area×20 mm), plaque volume (PV; mm^3) (vessel volume minus lumen volume), and % PV (PV/average vessel volume)×100. Plaque progression was assessed as the Δ% PV (difference between 6 and 3 months % PVs). Virtual histological IVUS analysis color coded tissue as dark green (fibrous tissue), light green (fibrofatty tissue), red (necrotic core), or white (dense calcium).

Subsequently, the IVUS catheter was replaced with a 2.7F OCT catheter (C7 DragonFly; St Jude Medical, St Paul, MN) to record OCT images from the mid- to distal LAD artery at an automatic pullback speed of 20 mm/s (100 frames/s), with blood clearance by infusion of contrast media. Images were analyzed offline by LightLab imaging (C7-XRTM system; St Jude Medical).[46,47] An atherosclerotic plaque was defined as a mass lesion (focal thickening) or loss of a layered structure of the vessel wall.[48] To coregister a lesion location between initial and follow-up IVUS and OCT studies, anatomical landmarks, such as side branches or calcifications, were used.

Micro-CT

To evaluate the myocardial microcirculation, an intravascular contrast (microfil; Flow Tech Inc, Tempe, AZ) was perfused into the myocardial microvessels under physiological pressure through a cannula ligated in a branch of the left circumflex coronary artery (LCX). The transmural myocardium was scanned with an in-house micro-CT at a 20-µm resolution. The spatial density, average diameter, and tortuosity of

microvessels (diameters, 20–500 µm) in the subepicardium and subendocardium were analyzed using ANALYZE, as described.[49]

Histopathological Analysis

After euthanasia, the hearts were harvested, and the coronary arteries were perfusion fixed and subsequently removed and sectioned at 3- to 5-mm intervals, with the most proximal segment offset in the block for paraffin embedding with section orientation. Segments were dehydrated and paraffin embedded for histological studies, and 1 to 7 sections were obtained from the ostium, proximal, middle, and distal portions of each coronary artery. Because of variation in artery length, we typically had 1 to 3 sections for left main artery and 6 to 7 sections each for proximal, middle, and distal LAD, LCX, or right coronary artery (RCA). Heart tissue was sliced (1–1.5 cm) parallel to the posterior atrioventricular sulcus, and myocardial sections were sampled at the midlevel circumferentially to include the anterior, lateral, posterior, and septal walls and right ventricle. Tissues were stained with Movat's pentachrome to highlight connective tissue, hematoxylin and eosin to confirm lesion details, and von Kossa to demonstrate calcium deposits; they were examined by an experienced pathologist (F.D.K) using light microscopy. Coronary arteries were also stained with Sirius red. Immunohistochemistry was performed in paraffin-embedded sections. Rabbit anti-CD31 polyclonal antibody (1:100 dilution; ab28364; Abcam), mouse anti-CD107a monoclonal antibody (1:400 dilution; MCA2315GA; AbD Serotec), mouse anti–smooth muscle actin monoclonal antibody (1:200 dilution; M0851; Dako), and mouse anti-oxidized phospholipid antibody (1:100 dilution; E06 antibody 330001; Avanti) were used as primary antibodies. The immunohistochemical staining was developed and visualized by using EnVision+ kit (Dako) and NovaRED kit (Vector Laboratories). The images were captured by Axio Scan Z1 (Zeiss, Germany) using a ×20 objective, and figures were prepared on the HALO image analysis platform (Indica Labs, Corrales, NM). Positive immunostaining for CD107a and smooth muscle actin and the percentage of stenosis were quantified in representative images. Sirius red staining images taken on BX51 Olympus microscope under polarized light were also used for collagen quantification.

Lesion types were grouped as advanced lesions (fibrofatty or fibroatheroma), early lesions (intimal thickening and xanthoma), or normal.[50] Briefly, early lesions, composed of smooth muscle cells and macrophage-derived foam cells in the intima, are recognized by intimal thickening and fatty streaks. Advanced lesions, designated as fibrofatty or fibroatheroma, are typically characterized by a necrotic core with a fibrous cap, which consist of less cholesterol and lipid-laden cells, matrix, cellular debris, and more foamy cell at the periphery of plaque and focal calcification on its base. The fibroatheromas have significant necrotic core, whereas the fibrofatty lesions have small sporadic necrosis, cholesterol clefts, and sometimes calcification. The average percentage of lesion number per all coronary artery sections was compiled for each pig. Sirius red myocardial staining was assessed by average percentage of staining/field (AxioVision 4.8.2; Carl Zeiss Microscopy, Thornwood, NY).[39]

Statistical Analysis

Statistical analysis was performed using the JMP software package, version 13.0 (SAS Institute, Cary, NC). All available data are included in the analyses presented. Analyses of change between study time points were performed using repeated measurements analyses by matched pairs or standard least squares linear regression, as appropriate. Normally distributed data are expressed as mean±SD, with variance of means by study group analyzed by 1-way ANOVA, and where significant, all pair comparisons of means were done using Tukey-Kramer honestly significant difference method. Nonnormally distributed data are expressed as median and range, with variance analyzed by Kruskal-Wallis rank sums testing, and where significant, all pair comparisons of means were done using Dunn method for joint ranking. Analyses of variance were done using α=0.05. Specific analyses are as indicated in figure or table legends.

Results

PCSK9 GOF Model Development

The primate coding sequence for *PCSK9* (*Pan troglodytes*, 99% identical to *Homo sapiens*), containing the mutation causing D374Y substitution, was inserted into a *Sleeping Beauty* transposon under the direction of a liver-specific promoter (Figure 1A). The transgene cassette was then introduced into male Ossabaw and Landrace fibroblasts using a transposon coselection strategy[30] (Figure 1A), and multiple integration events were identified by Southern blotting (data not shown) and verified by sequencing (Figure 1B). Ectopic PCSK9 protein was present in serum of *PCSK9* GOF and absent in controls (Figure S1A). Western blotting of liver protein extracts confirmed the reduction in LDL receptor protein as a result of the *PCSK9-D374Y* transgene expression (Figure S1B).

Evaluation of Breed-Specific Founders

PCSK9 GOF founders were raised on a standard swine diet, and they were compared with standard diet-fed cloned wild-type swine. Irrespective of breed background, founders had apparent elevations in blood TC, LDLc, total triglycerides, and
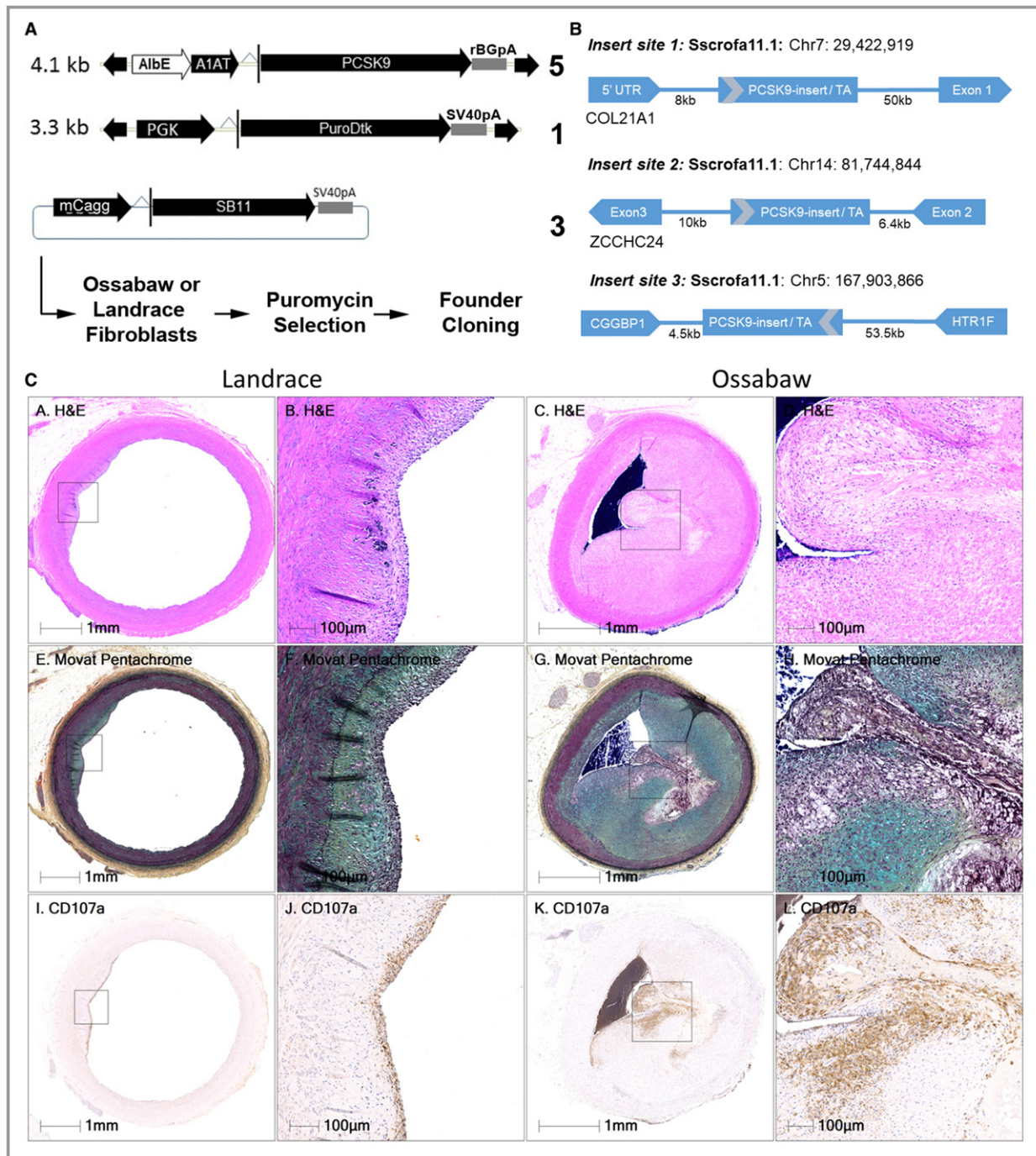
Figure 1. Development and histopathological analysis of Ossabaw and Landrace founders. A, A schematic of the *Sleeping Beauty* transposon used to generate pigs with ectopic expression of chimpanzee (*Pan troglodytes*) PCSK9 (proprotein convertase subtilisin-like/kexin type 9) from the liver-specific fusion promoter, consisting of the murine albumin enhancer (AlbE) and human α-1 antitrypsin promoter (A1AT). B, Insertion sites of the PCSK9 transgene mapped in the Ossabaw founder. C, Representative images of plaques in the left anterior descending artery of Landrace and Ossabaw founders (A through L). The Landrace founder shows minimally occlusive lesions with neointimal hyperplasia and mild inflammation near the vessel lumen, whereas the Ossabaw founder shows an advanced, complex, highly occlusive lesion with extensive inflammation. Ages are 14 and 15 months for Landrace and Ossabaw, respectively. A through D, Hematoxylin & eosin (H&E). E through H, Modified Movat's pentachrome. I through L, Immunohistochemistry staining for CD107a, highlighting inflammation. Chr indicates chromosome; mCagg, mini Caggs promoter; PGK, phosphoglycerate kinase promoter; PuroDK, puromycin-(delta)thymidine kinase; rBGpA, rabbit beta-globin polyadenylation sequence; SV40pA; simian virus 40 polyadenylation sequence; UTR, untranslated region.

Table 1. Fasting Blood Lipid Measurements in PCSK9 GOF Founders Receiving Standard Diet

Group	Blood Lipids, mg/dL				
	TC	LDLc	HDLc	TG	VLDL-TG
Control Landrace (n=2)	75.5±2.1	38.5±7.8	34.5±9.2	28.5±6.4	13±4.2
Landrace PCSK9 GOF (n=2)	224.5±64	167.5±46	22±4.2	133.5±54.4	69.5±30.4
Ossabaw PCSK9 GOF (n=1)	269	204	27	165	74

Data are given as mean±SD. Lipid measurements were made using nuclear magnetic resonance; no statistics were done because of low number of animals for comparison. GOF indicates gain of function; HDLc, high-density lipoprotein cholesterol; LDLc, low-density lipoprotein cholesterol; PCSK9, proprotein convertase subtilisin-like/kexin type 9; TC, total cholesterol; TG, triglyceride; VLDL, very-low-density lipoprotein.

very-LDL–associated (VLDL) triglycerides compared with unmodified controls (Table 1). Concordant with elevated LDLc and VLDL triglyceride concentrations, LDL and VLDL particle concentrations were increased in founder blood compared with controls (Table S1). Founders also had apparent decreases in high-density lipoprotein (HDL) cholesterol and HDL particle concentrations. The mean particle sizes of VLDL and HDL in founders were decreased and increased, respectively.

Microscopic histopathological examination of the coronary vessels at 14 months in Landrace founder animals revealed early atheromas. In contrast, the coronary vessels in the 15-month-old Ossabaw founder (No. 1513) revealed advanced atherosclerotic disease, despite similar profiles of dyslipidemia. Coronary lesions in the Ossabaw founder showed significantly stronger inflammation, revealed by immunostaining for CD107a that highlights inflammatory macrophages highly expressing lysosome–associated membrane protein 1, compared with that observed in the Landrace founder (Figure 1C and Figure S2). Histopathological features revealed nearly occlusive plaques in each of the major coronary arteries of the Ossabaw founder, with estimates of stenosis reaching 70% to 90%. Because the benefits of Ossabaw genetics, specifically more severe phenotype and small stature, outweigh the superior fecundity of Landrace, further study was continued with only Ossabaw swine.

Disease Course in Ossabaw Cloned Progeny

To characterize atherosclerosis progression in Ossabaw PCKS9 GOF animals and determine if atherogenic diet would accelerate disease, clones of the Ossabaw founder (No. 1513) were randomized into 2 groups (n=7 per group). Starting at 3 months of age, Ossabaw PCSK9 GOF animals were fed either a standard or atherogenic diet, and compared with standard diet fed, age-matched, unmodified Ossabaw swine clones (n=7) at 6 and 9 months of age. Both PCSK9 GOF groups had marked dyslipidemia (Table 2). Significant elevations of TC and LDLc were measured in both PCSK9 GOF groups and at all time points compared with controls. The

atherogenic diet induced further significant increases in TC, LDLc, and HDL cholesterol in these animals at both 6 and 9 months age. The LDL:HDL ratio changed from ≤1.0 in the controls to >5.0 for all model animals, irrespective of diet. In contrast to the founder, only sporadic increases in triglycerides were measured in the PCSK9 GOF animals compared with controls. At 6 months of age, PCSK9 GOF animals consuming the standard diet had a statistically significant increase in triglycerides compared with age-matched controls (P=0.0373). There were no significant correlations between age and triglycerides in controls or PCSK9 GOF animals. However, there was a moderate positive correlation between TC and age in PCSK9 GOF atherogenic animals (R^2=0.28). Although the effect of age on triglycerides was significant

Table 2. Fasting Blood Lipid Measurements From Characterization Study

Age, mo	Value, mg/dL			
	TC	LDL	TG	HDL
Ossabaw control				
3	78.7±23.1	36.3±21.0	29.8±10.0	36.3±2.3
6	76.7±24.5	32.1±15.5	25.3±19.9	39.6±6.5
9	83.7±20.9	29.9±12.6	34.6±29.0	47.0±13.4
Ossabaw, PCSK9 GOF				
3	293.0±22.0*	250.1±17.4*	31.7±10.7	36.4±4.2
6	466.7±214*	412.0±195*	48.0±14.7[†]	45.1±19.9
9	434.4±47.2*	388.7±45.8*	40.3±13.5	37.6±3.9
Ossabaw, PCSK9 GOF ATH				
3	345.0±67.9*	295.7±60.1*	40.0±13.0	41.3±8.0
6	857.6±143*,[‡]	769.4±121*,[‡]	38.9±11.5	80.3±25.3*,[‡]
9	952.1±176*,[‡]	853.6±161*,[‡]	57.6±10.1[†]	87.1±20.8*,[‡]

ATH indicates atherogenic; GOF, gain of function; HDL, high-density lipoprotein; LDL, low-density lipoprotein; PCSK9, proprotein convertase subtilisin-like/kexin type 9; TC, total cholesterol; TG, triglyceride.

*P≤0.0008 compared with control.

[†]P<0.05 but P>0.01 compared with control; N=7 animals per group. Analysis was 1-way ANOVA, followed by Tukey-Kramer comparison.

[‡]P≤0.0027 compared with PCSK9 GOF Ossabaw receiving standard diet.

(P<0.0159) in this group, the effect of diet must also be considered. A multiple regression analysis of age and diet using pooled PCSK9 data showed a stronger effect of age than diet, but neither factor was significant using this approach.

Cardiac Structure and Function

All groups had significantly different mean body weights at both study time points, and the *PCSK9* GOF animals gained a larger relative percentage of weight between the study time points (P=0.001 for standard and P=0.0003 for atherogenic). Mean heart rate and blood pressures recorded by telemetry were stable during the course of the study and similar between all groups at both time points (Table S2). However, sedated heart rates for *PCSK9* GOF animals at 9 months of age were significantly increased over ambulatory age-matched baselines. A similar change was not observed in the control group (Table S2). End systolic volume was stable over the course of the study, and significantly lower mean end systolic volume in both *PCSK9* GOF groups compared with controls (P<0.0086) can be attributed to differences in body weight. End diastolic volume (EDV) and LV mass (LVM) increased from 6 to 9 months of age only in the *PCSK9* GOF groups, irrespective of diet (Table S2). Overall, EDV and LVM correlate with body weight at 6 months (EDV: R^2=0.32/P=0.0074; LVM: R^2=0.23/P=0.0293), but not at 9 months, of age. Because both EDV/LVM and body weights changed differentially, correlations between absolute difference in EDV or LVM and percentage of body weight gained between 6 and 9 months of age were examined. Only EDV in the control group positively correlated with body weight using this approach (R^2=0.66/P=0.0266). As a result, it would seem that increased EDV/LVM over time in *PCSK9* GOF animals is not entirely attributable to body weight gain. Screening for multiple interacting factors, including EDV or LVM (as appropriate), body weight, age, diet, and sedated heart rate, for effect by genotype, showed a strong positive correlation between LVM and EDV in the *PCSK9* GOF animals that is not observed in the controls (P<0.0001). The effect of diet was also significant in these analyses, but only when compared with LVM (P=0.0428). Although stroke volume, ejection fraction, and cardiac output tended to decrease from 6 to 9 months of age in controls, increases over time in EDV and higher sedated heart rate resulted in significant increases in the *PCSK9* GOF animals (pooled *PCSK9* GOF animals; systolic volume, P<0.0001; ejection fraction, P=0.0002; cardiac output, P=0.0011). Increases in ejection fraction for standard diet group and cardiac output for atherogenic diet group reached statistical significance in between-group comparisons (Table S2). Myocardial fibrosis was more prevalent in *PCSK9* GOF receiving atherogenic diet compared with controls (Figure S3). Spatial densities of subendocardial and subepicardial microvessels (0.2–0.5 mm) were also increased in 9-month-old PCSK9 GOF, irrespective of diet (Figure 2).

In Vivo Coronary Imaging

Sensitive in vivo imaging modalities will be important for evaluating new drugs targeted at every stages of atherosclerosis development. To determine whether we could detect early and progressing lesions, we imaged the LAD using IVUS and OCT. As expected, no atherosclerotic lesions were observed in control animals at any time point; however, lesions were readily detectable in the *PCKS9* GOF groups. In the *PCSK9* GOF consuming a standard diet, 43% and 100% of the animals had OCT-detectable lesions at 6 and 9 months of age, respectively, whereas 100% animals receiving atherogenic diet had detectable lesions at both time points. Percentage PV measured by IVUS increased over time in all groups and reached statistical significance for PCSK9 GOF atherogenic group (Figure 3B). By 9 months age, both PCSK9 GOF groups had significantly elevated percentage PV compared with age-matched controls (Figure 3A). Virtual histological IVUS done at 9 months of age showed that 100% of the PCSK9 GOF animals had lesions containing a detectable necrotic core, and 9 of 13 of these animals also had dense calcification (Figure 3C and 3D). Compared with control group, medians for all plaque components increased for both PCKS9 GOF groups at 9 months of age. Necrotic core was significantly increased in both PCSK9 GOF groups, fibrous plaque was significantly greater in the atherogenic group, and fibrofatty plaque was significantly greater in the standard diet group. Hence, IVUS and OCT studies are effective for detecting early disease and provide measurable outcomes in follow-up compared with baseline.

Lesion length (LL) and percentage DS of coronary lesions are important metrics for designing preclinical studies for stents or atherectomy devices. Accordingly, we used CTA to measure LL and DS in the LAD, LCX, and RCA at 6 and 9 months of age. No significant lesions were detected in the control group. At 6 months of age, irrespective of diet, PCSK9 GOF animals had sporadic detectable lesions in the proximal and middle segments of the LAD and RCA, but DS was low (<10%) (data not presented). At 9 months of age, PCSK9 GOF animals consuming standard diet had detectable lesions that were most prevalent in the proximal segments, but were also detected in the middle segment of the LAD (Figure S4). The maximal DS in these segments was 17% to 19%, with a maximal LL of 6.8 to 8.6 mm. At 9 months of age, the atherogenic diet group had 100% prevalence of detectable lesions in the proximal segments of the LAD and RCA, and all but 1 animal had lesions in the middle segment of the RCA. Mean DS and LL were higher in animals consuming
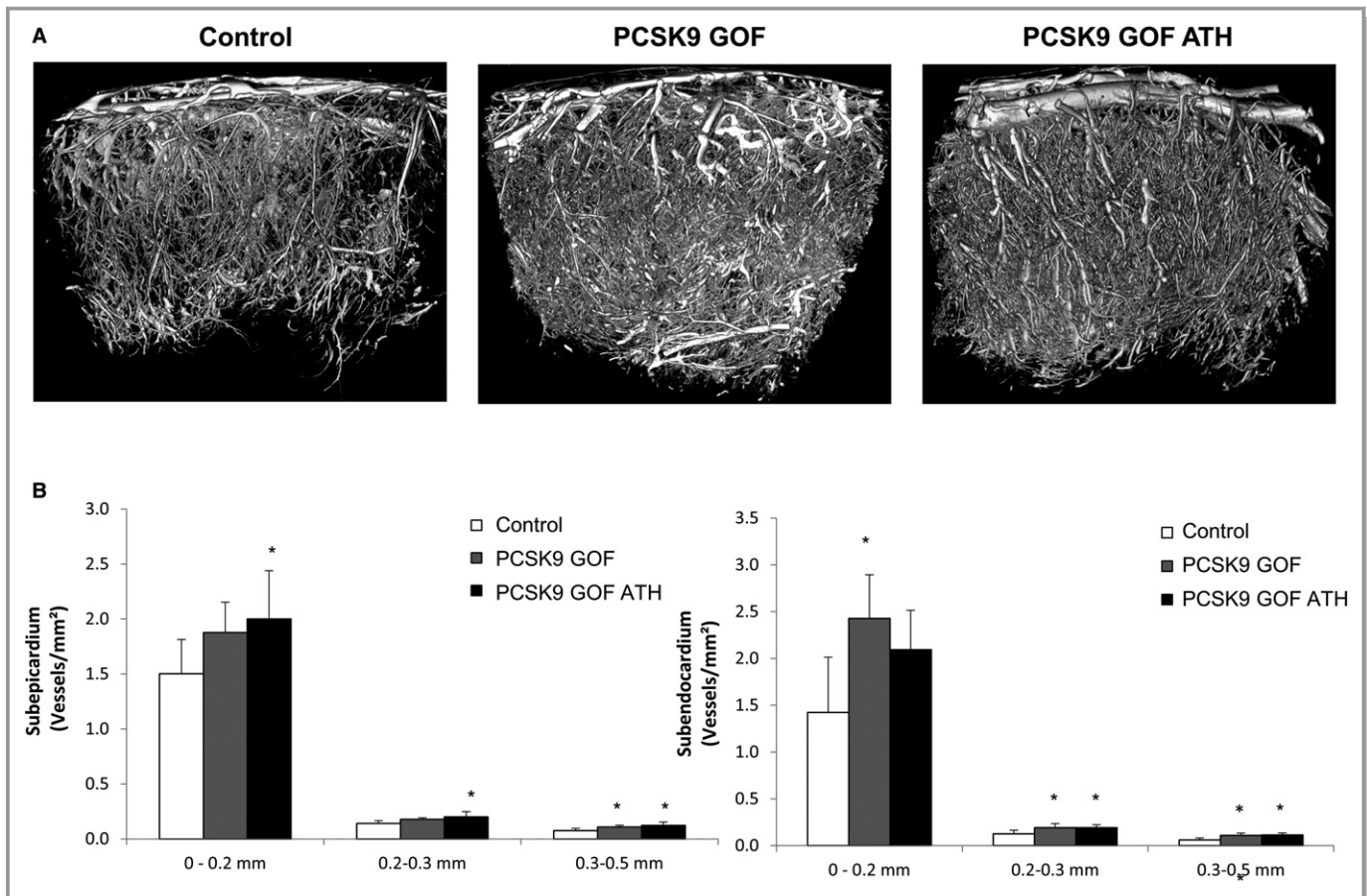
Figure 2. Representative micro–computed tomography (CT) images of myocardial vessels. A, Representative micro-CT images from the characterization study showed vessel density is higher in gain-of-function (GOF) animals. B, Spatial density of subepicardial and subendocardial microvessels was variously increased in both model groups. Means and SDs shown. *$P<0.05$ compared with control using 1-way ANOVA testing, followed by comparisons for all pairs using Tukey-Kramer honestly significant difference method. ATH indicates atherogenic; PCSK9, proprotein convertase subtilisin-like/kexin type 9.

atherogenic diet in all segments, except the middle LCX. Increases in DS for the proximal LAD and middle RCA, as well as LL for proximal RCA, reached statistical significance ($P<0.05$) compared with PCSK9 GOF animals consuming standard diet. The maximal DS in these additional segments was 18% to 37%, with a maximal LL of 9.9 to 38.3 mm. Hence, PCSK9 GOF animals had increased lesion development over time, and consumption of the atherogenic diet increased lesion progression.

Microscopic Histological Analysis

At the summation of the study, we conducted histopathological analysis of the hearts from all groups to corroborate the findings from in vivo imaging studies. Compilation of all findings from all artery sections screened (Figure 4A through 4C) shows that in the control group, sections were predominantly normal, with early lesions found in 30% of sections. Overall in PCSK9 GOF groups, sections show more advanced lesions, including a smaller fraction of calcified lesions (Figure 4A through 4C). In the PCSK9 GOF group consuming atherogenic diet, 80% of sections revealed advanced lesions, with 10% of those showing calcification. Breakdown of these data by vessel type shows that the addition of the atherogenic diet increased the frequency of advanced lesions observed in the LCX and the frequency of calcification in all coronary arteries. Lesions in the RCA and LAD of PCSK9 GOF animals generally represent significant fibrofatty or fibroatheromatous plaques with necrosis and an overlying fibrous cap, as well as occasional intimal calcification highlighted by speckled to dense von Kossa staining (Figure 5 and Figure S5). Fibroatheromas (with necrotic cores) were observed in both the RCA and LAD of nearly every PCSK9 GOF atherogenic animal (specifically, 5 of 6 in the RCA and 6 of 6 in the LAD). All PCSK9 GOF arteries examined in this study, including the 14-month-old Landrace founder, had pronounced immunohistochemical staining for CD107a, particularly in the arterial intima, highlighting activated macrophages (Figures 1 and 6
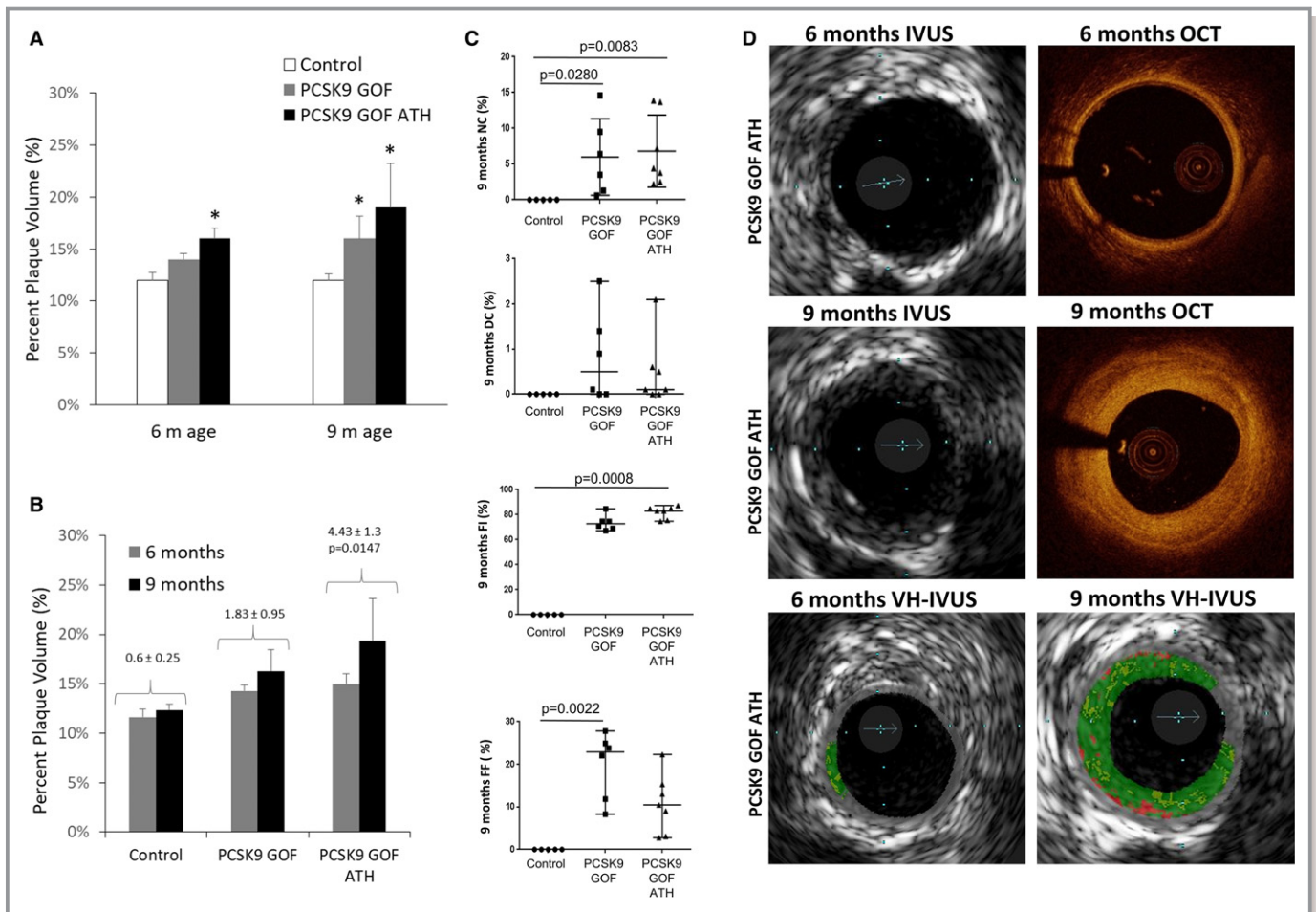
Figure 3. In vivo lesion characterization. A, Percentage plaque volume measured by intravascular ultrasound (IVUS) was higher in the left anterior descending artery (LAD) of both model groups compared with controls. Means and SDs shown. *$P<0.05$ compared with Control using 1-way ANOVA testing, followed by comparisons for all pairs using Tukey-Kramer honestly significant difference method. B, Percentage plaque volume measured by IVUS also increased longitudinally in the LAD of both model groups. Mean±SD shown. Significance of mean differences, determined from matched-pair analyses by study group, is noted, and post hoc 2-tailed *t* tests showed that only the *PCSK9* (proprotein convertase subtilisin-like/kexin type 9) gain-of-function (GOF) atherogenic (ATH) group had statistically increased plaque volume over time. C, At 9 months age, all coronary plaque components by virtual histological IVUS were increased in model animals compared with control. Mean and SDs shown. Kruskal-Wallis tests, followed by nonparametric comparisons for all pairs using Dunn method for joint ranking, revealed various component increases reached statistical significance, although these results are limited by this conservative approach because of missing data points. D, Corresponding IVUS and optical coherence tomography (OCT) images at the same coronary segment demonstrate longitudinal plaque progression. DC indicates dense calcification; FF, fibrofatty; FI, fibrous; NC, necrotic core.

and Figures S2 and S6). All lesions in the control group lack CD107a^{+} and represent minimal neointimal thickening, consisting mainly of smooth muscle cells and proteoglycans, with rare foam cells (Figure 6 and Figure S6). In contrast, CD31 immunostaining, highlighting endothelial cells expressing platelet endothelial cell adhesion molecule, was similar in most PCKS9 GOF animals to that seen in controls, where expression was mostly limited to the luminal vascular endothelial cell lining; however, sporadic positive cells in the intima were in some of the most advanced lesions highlighting intraplaque angiogenesis (indicated vasa vasorum, Figure 6). E06 antibody immunostaining for oxidized phospholipid

showed no increased accumulation of oxidized LDL in PCSK9 GOF animals versus controls.

Discussion

This study describes the initial characterization of a novel atherosclerosis model produced by pairing genome-engineering technology with Ossabaw genetics. Data from founder animals in this study show that a combination of the *PCSK9* GOF transgene with susceptible Ossabaw breed distinctly enhances features consistent with atherosclerosis compared with the same transgene in conventional swine. Without
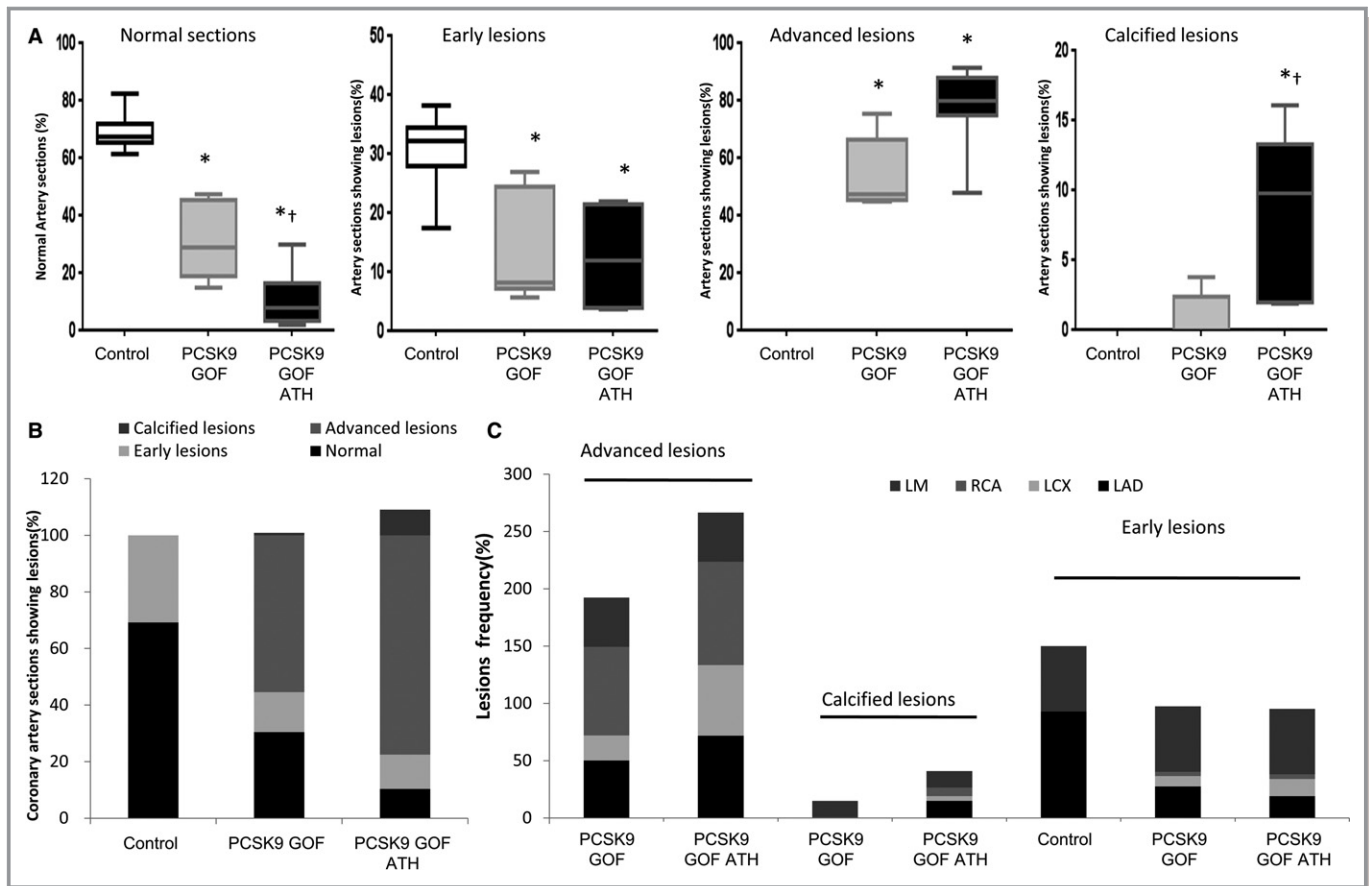
Figure 4. Quantification, classification, and distribution of atherosclerotic lesions by histopathologic analysis. A, The median and range is expressed as the percentage of all coronary artery sections showing lesions in each group (left anterior descending artery [LAD], left circumflex coronary artery [LCX], left main coronary artery [LM], and right coronary artery [RCA] compiled). LAD, LCX, and RCA compiles proximal, mid, and distal from an average 16 sections per animal, per artery. LM was not subdivided, and the average number of sections per animal is 2. *$P<0.05$ compared with control; †$P<0.05$ compared with *PCSK9* (proprotein convertase subtilisin-like/kexin type 9) gain of function (GOF) receiving standard diet by Kruskal-Wallis tests, followed by nonparametric comparisons for all pairs using Steel-Dwass method. B, The distribution of atherosclerotic lesion type in all groups. C, The distribution of advanced, calcified, and early atherosclerotic lesion types in each coronary artery in all groups (compiled, of 100% per artery). Advanced and calcified lesions were not observed in controls. ATH indicates atherogenic.

dietary challenge, PCSK9 GOF Ossabaw receiving standard diets have higher (up to 2-fold) plasma lipids than wild-type Ossabaw receiving HFHC diets. Both the PCSK9 GOF Ossabaw and wild-type Ossabaw develop atherosclerosis, although the time frame is nearly half for the PCSK9 GOF animals (24 versus 43 weeks).[21,51] Unlike the HFHC-fed Ossabaw in previous studies, we do not expect Metabolic syndrome (MetS) in our PCSK9 GOF animals receiving standard diet. Notably, without HFHC or MetS induction, PCSK9 GOF pigs consistently, 100% by 9 months of age, develop moderate atherosclerosis. This suggests MetS is not required for atherogenesis in the Ossabaw background and enables performing preclinical testing of treatments for early atherosclerosis and/or prevention without HFHC diets or MetS.

The Ossabaw model produces dyslipidemia consisting of increased LDLc and triglycerides to a level similar to humans with familial hypercholesterolemia. Consumption of an atherogenic diet amplifies the combined hyperlipidemia phenotype. In humans, high triglycerides (>150 mg/dL), low HDL cholesterol (<50 mg/dL in women, <40 mg/dL in men), and increased prevalence of small dense LDL particles constitute atherogenic dyslipidemia that is associated with cardiovascular disease in patients with metabolic syndrome and type 2 diabetes mellitus.[52] Likewise, studies have demonstrated reduced glucose tolerance and insulin binding/affinity in Ossabaw compared with Yorkshire swine and concluded that Ossabaw swine possess a natural insulin resistance.[53,54] Although lipoprotein particle size was only measured in founders, it is interesting that, compared with nonmodified pigs measured at the same time in the same laboratory, triglyceride concentration was increased in both Ossabaw and Landrace, HDL concentration was decreased, and VLDL particle size was smaller (Table S1).
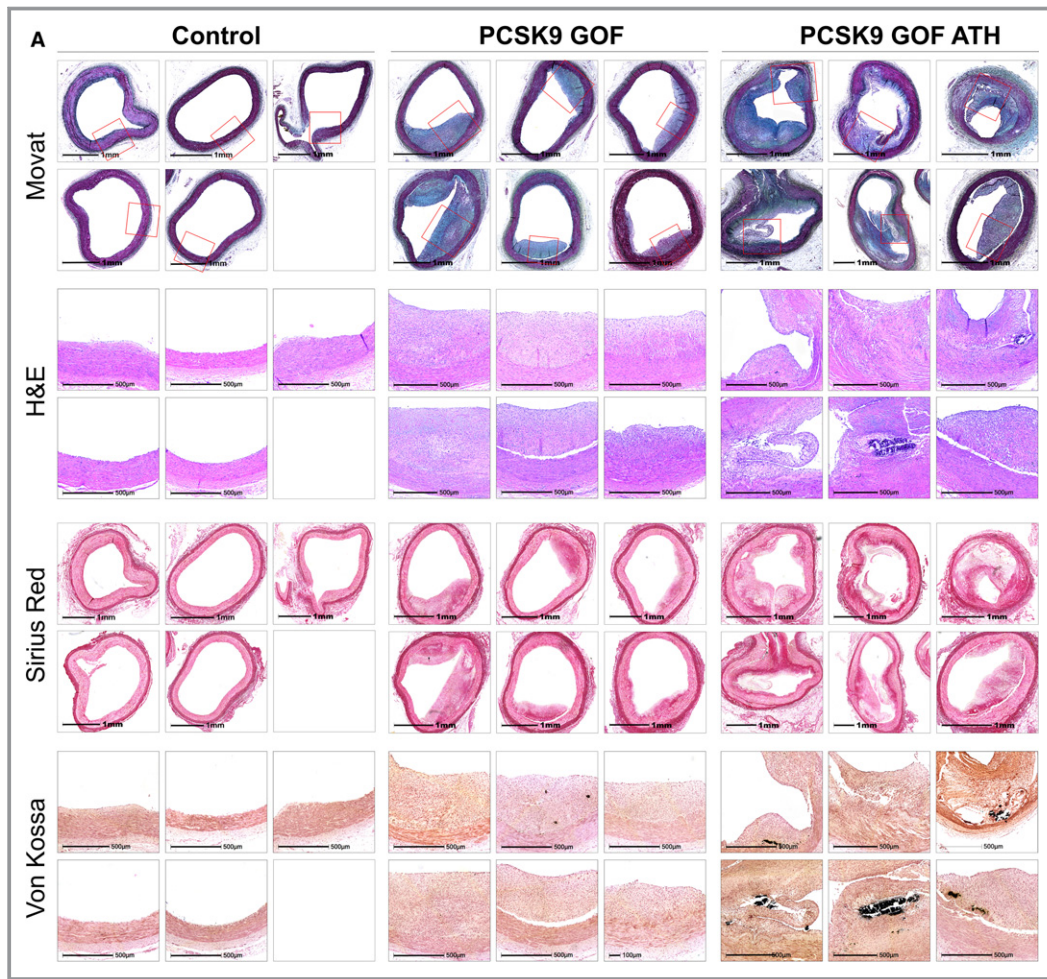
Figure 5. Histopathological features of plaques in the right coronary artery (RCA). Representative histopathological features of the most stenotic section of the proximal RCA in each subject: control (n=5), *PCSK9* (proprotein convertase subtilisin-like/kexin type 9) gain of function (GOF) (n=6), and PCSK9 GOF atherogenic (ATH) (n=6). A, The higher-power magnifications (hematoxylin and eosin [H&E] and von Kossa stains) represent regions corresponding to the red box in the low-power Movat's pentachrome stain. Histologic coronary staining top to bottom: modified Movat's pentachrome, H&E, picrosirius red, and von Kossa (highlighting calcium). Bar: low-power image=1 mm; higher-power image=500 μm. B, Sirius red staining images taken on BX51 Olympus microscope under polarized light were used for collagen quantification; the percentage of stenosis was also quantified in the displayed images. Values displayed are means and SDs. Calcification area in plaque and percentage of plaque area were quantified from the displayed von Kossa stained images. Calcification data were analyzed by Kruskal-Wallis testing, followed by Dunn's multiple comparison. Median±interquartile values displayed. *P<0.05 compared with control; †P<0.05 compared with PCSK9 GOF receiving standard diet using 1-way ANOVA, multiple comparison analysis.

Indeed, others have realized the value of modeling atherosclerosis with naturally occurring mutations, knockout of *LDLR* or transgenic expression of *PCSK9-D374Y*, and have showed significant elevations in total and LDLc.[1,4,5,55] Unlike Ossabaw, the Yucatan and conventional pigs do not develop MetS when challenged with HFHC diet, and lesion formation in the Yucatan PCSK9 GOF pigs is not increased by chemically induced diabetes mellitus type 1.[55] Although this recent development of models demonstrates an unmet need in preclinical modeling, widespread access to these models is

significantly limited geographically by International Animal Product Export Regulations.

The current study shows that this new model does not require diet modification or overt injury to develop atherosclerotic coronary lesions detectable by OCT, IVUS, and CTA. PCSK9 GOF animals in this study, irrespective of diet, developed lesions predominantly in the LAD and RCA, with similar pathophysiological characteristics and distribution to those seen in humans.[50] Longitudinal evaluation by in vivo imaging can track disease development from early
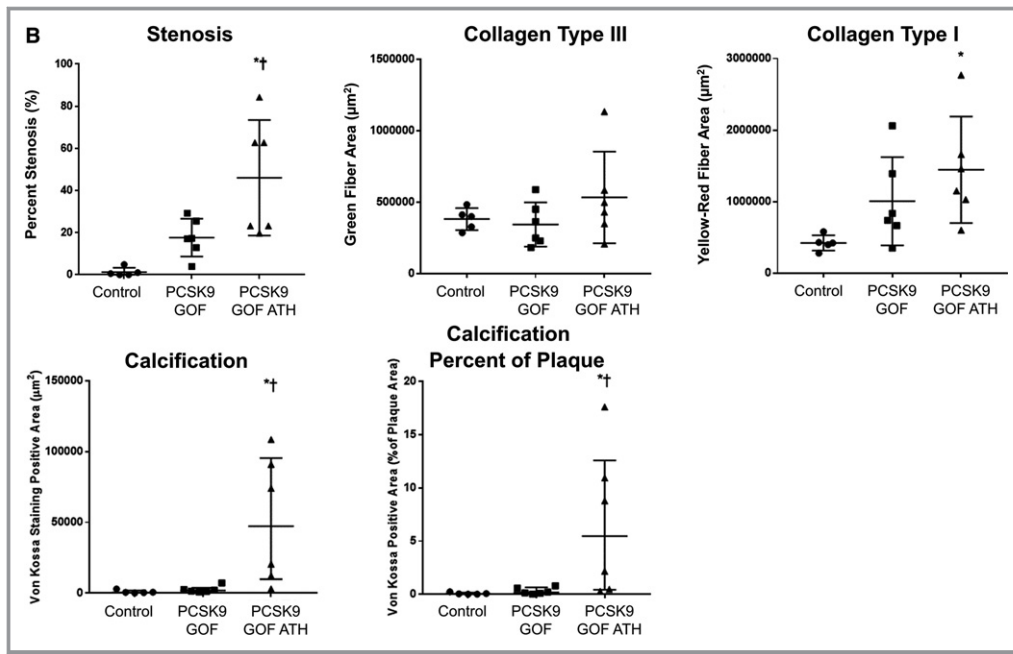
Figure 5. Continued

states to more progressive lesions; this is ideal for testing drugs that affect early-stage atheroma development. Consumption of an atherogenic diet accelerates the rate and consistency of lesion development and produces more advanced coronary lesions that are multifocal and diffuse, similar to those seen in human disease progression, with consistent presence of inflammation, fibrosis, necrotic cores, and sporadic calcification. Histopathological analysis corroborates these results, but the degree of stenosis observed in tissue sections exceeds that observed by CTA or IVUS/OCT, likely because of tissue processing and/or outward remodeling. In humans, macrophages are present in the arterial intima early in atherosclerosis and accumulate with advancing disease. This is consistent with the pattern of CD107a^{+} macrophage staining in the arterial intima, irrespective of diet, from all PCSK9 GOF lesions, coronary arteries, examined in this study. The macrophage staining in the intima also appears to be more pronounced as lesions progress to more advanced stages. Despite some early lesion formation in control animals detected by IVUS and histological analysis, no macrophage staining was observed in these arteries nor was virtual histological IVUS able to detect features of more advanced lesions. In addition, the PV measurement by IVUS is prone to overestimation compared with histological analysis, which includes the media.[56] This suggests that macrophage activation is an inherent feature of PCSK9 GOF that is enhanced by consumption of an atherogenic diet. PCSK9 GOF animals also developed mild LV hypertrophy and fibrosis and myocardial microvascular neovascularization,

which is possibly secondary to the chronic inflammation observed.[57,58]

Myocardial metabolic dysfunction may lead to LV remodeling and diastolic dysfunction, attributed to the lipid-related mitochondrial dysfunction and oxidative stress.[59] The PCSK9 GOF animals also developed mild LV hypertrophy and fibrosis by 9 months of age. The observed myocardial microvascular neovascularization in model animals is consistent with the effect of hypercholesterolemia,[57,58] possibly secondary to oxidative stress and inflammation, and consequent release of cytokines and growth factors.[60] This may have also accounted for myocardial fibrosis observed in the model animals. Last, both the PCSK9 GOF and PCSK9 GOF atherogenic groups had increases in EDV and LVM over time that were highly correlated, not entirely attributable to changes in body weight and not observed in controls. These data could be explained by decreased ventricular compliance because of the development of myocardial fibrosis and increased angiogenesis and/ or reduced ventricular filling time because of the increased heart rate under anesthesia compared with baseline in the 9-month-old PCSK9 groups.

Limitations

IVUS and OCT were only performed in the proximal 20-mm segment of the LAD, which ultimately had fewer lesions than the RCA and, therefore, cannot be comprehensively compared with histopathological analysis. Furthermore, the relative lower spatial resolution of MDCT (0.5 mm) may limit its
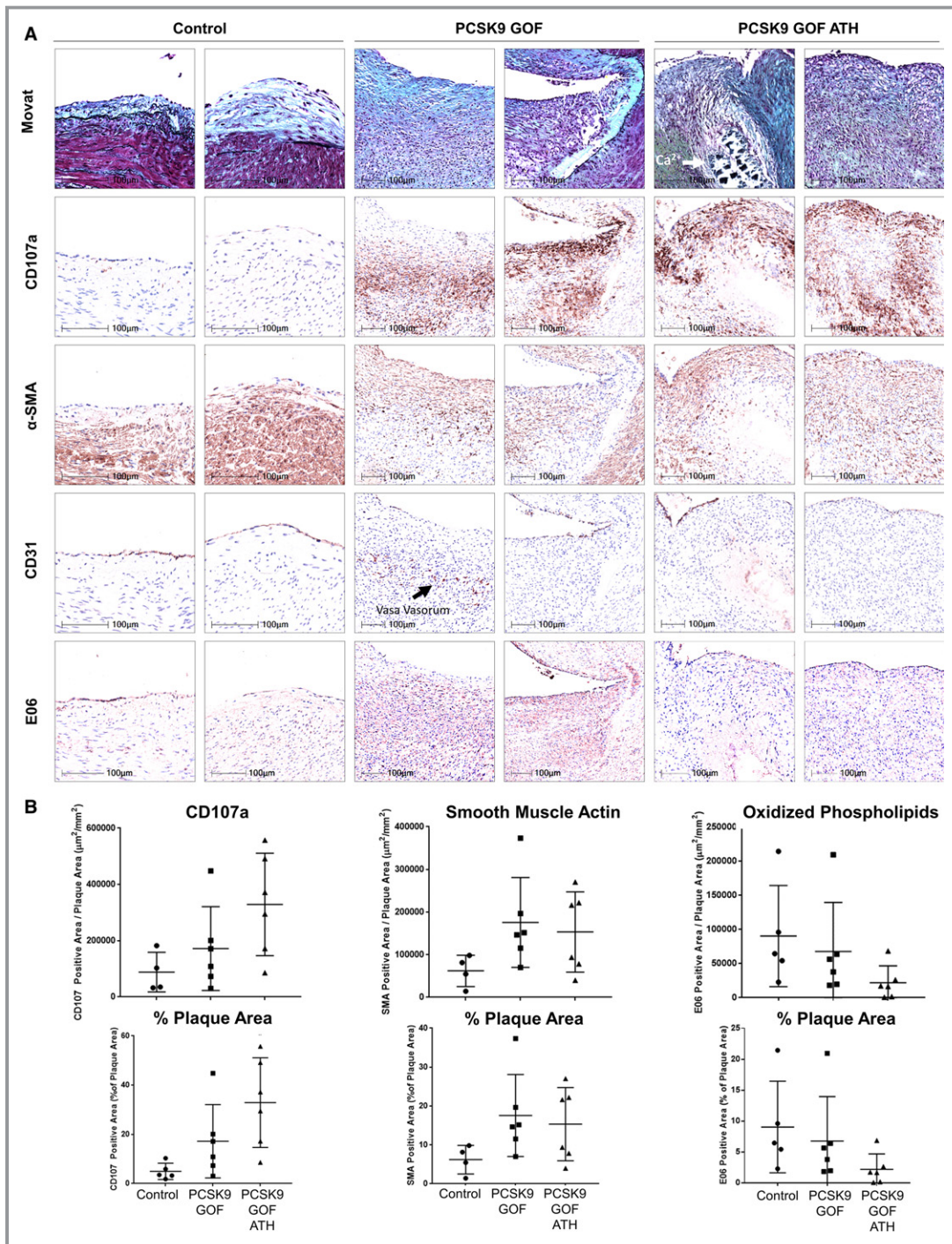
Figure 6. Immunohistochemical analysis of plaques in the right coronary artery. A, Immunohistochemistry staining for CD107a, α-smooth muscle actin (α-SMA), CD31, and E06 highlights inflammation, neointimal hyperplasia, endothelial cells, and oxidized phospholipids, respectively, predominantly in gain-of-function (GOF) groups. B, CD107a, α-SMA, and E06 immunostaining areas were quantified on HALO platform (Indica Labs, Corrales, NM), and results were presented as total CD107a- or α-SMA–positive area per plaque area and the percentage of plaque area. Mean and SD are displayed. *$P<0.05$ compared with control; [†]$P<0.05$ compared with proprotein convertase subtilisin-like/kexin type 9 (PCSK9) GOF receiving standard diet using 1-way ANOVA, multiple comparison analysis. ATH indicates atherogenic.

application in small-caliber segments, particularly for lesions with mild stenoses observed in our study.[61] In addition, CTA-based coronary arterial stenoses in vivo showed slight discrepancy from histological features, possibly because of arterial remodeling, shrinkage of tissue during fixation, and the limited duration of study.[46] The study also is limited by a short observation period and relatively mild stenoses; presumably, longer duration may induce more severe obstructive atherosclerotic lesions. The *PCSK9* cDNA used in this study was derived from chimp and codon optimized to pig. Because chimp and human PCSK9 are highly conserved (685/692 residues[62]), we expect most protein inhibitors will cross-react. Because of codon optimization, RNA interference therapy could be evaluated with custom targets, as demonstrated in rodents and nonhuman primates.[63] Last, we studied clones of founder animal 1513, whereas future supply will be descendants of 1513. Characterization of additional PCSK9 GOF alleles in inbred or outcrossed animals may provide alternative lines with a range of penetrance and kinetics of disease progression.

In conclusion, this study shows that superimposition of a PCSK9 GOF on the Ossabaw pig background provides a consistent and practical model of human coronary atherosclerosis. Ongoing work with a combined hyperlipidemia phenotype with dietary induction of metabolic syndrome may also be useful for attaining consistent advanced lesion development in the peripheral vasculature describing peripheral atherosclerotic lesions that have previously been difficult to produce. This would further add to the human disease relevance of this model, aligning with growing public health attention to the increasing incidence of cardiovascular disease linked to metabolic syndrome and type 2 diabetes mellitus.[64–67]

Acknowledgments

Sources of Funding

Disclosures

Melkamu, Fahrenkrug, and Carlson are employees and shareholders of Recombinetics, Inc. The remaining authors have no disclosures to report.

References

1. Rapacz J, Hasler-Rapacz J, Taylor KM, Checovich WJ, Attie AD. Lipoprotein mutations in pigs are associated with elevated plasma cholesterol and atherosclerosis. *Science*. 1986;234:1573–1577.

2. Thim T, Hagensen MK, Drouet L, Bal Dit Sollier C, Bonneau M, Granada JF, Nielsen LB, Paaske WP, Botker HE, Falk E. Familial hypercholesterolaemic downsized pig with human-like coronary atherosclerosis: a model for preclinical studies. *EuroIntervention*. 2010;6:261–268.

3. Tellez A, Krueger CG, Seifert P, Winsor-Hines D, Piedrahita C, Cheng Y, Milewski K, Aboodi MS, Yi G, McGregor JC, Crenshaw T, Reed JD, Huibregtse B, Kaluza GL, Granada JF. Coronary bare metal stent implantation in homozygous LDL receptor deficient swine induces a neointimal formation pattern similar to humans. *Atherosclerosis*. 2010;213:518–524.

4. Davis BT, Wang XJ, Rohret JA, Struzynski JT, Merricks EP, Bellinger DA, Rohret FA, Nichols TC, Rogers CS. Targeted disruption of LDLR causes hypercholesterolemia and atherosclerosis in Yucatan miniature pigs. *PLoS One*. 2014;9: e93457.

5. Li Y, Fuchimoto D, Sudo M, Haruta H, Lin QF, Takayama T, Morita S, Nochi T, Suzuki S, Sembon S, Nakai M, Kojima M, Iwamoto M, Hashimoto M, Yoda S, Kunimoto S, Hiro T, Matsumoto T, Mitsumata M, Sugitani M, Saito S, Hirayama A, Onishi A. Development of human-like advanced coronary plaques in low-density lipoprotein receptor knockout pigs and justification for statin treatment before formation of atherosclerotic plaques. *J Am Heart Assoc*. 2016;5:e002779.

6. Werner C, Hoffmann MM, Winkler K, Bohm M, Laufs U. Risk prediction with proprotein convertase subtilisin/kexin type 9 (PCSK9) in patients with stable coronary disease on statin treatment. *Vascul Pharmacol*. 2014;62:94–102.

7. Tomkin GH, Owens D. Investigational therapies for the treatment of atherosclerosis. *Expert Opin Investig Drugs*. 2014;26:1–11.

8. Chen SN, Ballantyne CM, Gotto AM Jr, Tan Y, Willerson JT, Marian AJ. A common PCSK9 haplotype, encompassing the E670G coding single nucleotide polymorphism, is a novel genetic marker for plasma low-density lipoprotein cholesterol levels and severity of coronary atherosclerosis. *J Am Coll Cardiol*. 2005;45:1611–1619.

9. Chernogubova E, Strawbridge R, Mahdessian H, Malarstig A, Krapivner S, Gigante B, Hellenius ML, de Faire U, Franco-Cereceda A, Syvanen AC, Troutt JS, Konrad RJ, Eriksson P, Hamsten A, van't Hooft FM. Common and low-frequency genetic variants in the PCSK9 locus influence circulating PCSK9 levels. *Arterioscler Thromb Vasc Biol*. 2012;32:1526–1534.

10. Huang CC, Fornage M, Lloyd-Jones DM, Wei GS, Boerwinkle E, Liu K. Longitudinal association of PCSK9 sequence variations with low-density lipoprotein cholesterol levels: the coronary artery risk development in young adults study. *Circ Cardiovasc Genet*. 2009;2:354–361.

11. Benjannet S, Rhainds D, Essalmani R, Mayne J, Wickham L, Jin W, Asselin MC, Hamelin J, Varret M, Allard D, Trillard M, Abifadel M, Tebon A, Attie AD, Rader DJ, Boileau C, Brissette L, Chretien M, Prat A, Seidah NG. NARC-1/PCSK9 and its natural mutants: zymogen cleavage and effects on the low density lipoprotein (LDL) receptor and LDL cholesterol. *J Biol Chem*. 2004;279:48865–48875.

12. Naoumova RP, Tosi I, Patel D, Neuwirth C, Horswell SD, Marais AD, van Heyningen C, Soutar AK. Severe hypercholesterolemia in four British families with the D374Y mutation in the PCSK9 gene: long-term follow-up and treatment response. *Arterioscler Thromb Vasc Biol*. 2005;25:2654–2660.

13. Leren TP. Mutations in the PCSK9 gene in Norwegian subjects with autosomal dominant hypercholesterolemia. *Clin Genet*. 2004;65:419–422.

14. Sun XM, Eden ER, Tosi I, Neuwirth CK, Wile D, Naoumova RP, Soutar AK. Evidence for effect of mutant PCSK9 on apolipoprotein B secretion as the cause of unusually severe dominant hypercholesterolaemia. *Hum Mol Genet*. 2005;14:1161–1169.

15. Timms KM, Wagner S, Samuels ME, Forbey K, Goldfine H, Jammulapati S, Skolnick MH, Hopkins PN, Hunt SC, Shattuck DM. A mutation in PCSK9 causing autosomal-dominant hypercholesterolemia in a Utah pedigree. *Hum Genet*. 2004;114:349–353.

16. Al-Mashhadi RH, Sorensen CB, Kragh PM, Christoffersen C, Mortensen MB, Tolbod LP, Thim T, Du Y, Li J, Liu Y, Moldt B, Schmidt M, Vajta G, Larsen T, Purup S, Bolund L, Nielsen LB, Callesen H, Falk E, Mikkelsen JG, Bentzon JF. Familial hypercholesterolemia and atherosclerosis in cloned minipigs created by DNA transposition of a human PCSK9 gain-of-function mutant. *Sci Transl Med*. 2013;5:166ra161.

17. Buhlinger CA, Wangsness PJ, Martin RJ, Ziegler JH. Body composition, in vitro lipid metabolism and skeletal muscle characteristics in fast-growing, lean and in slow-growing, obese pigs at equal age and weight. *Growth*. 1978;42:225–236.

18. Etherton TD. Subcutaneous adipose tissue cellularity of swine with different propensities for adipose tissue growth. *Growth*. 1980;44:182–191.

19. Etherton TD, Wangsness PJ, Hammers VM, Ziegler JH. Effect of dietary restriction on carcass composition and adipocyte cellularity of swine with different propensities for obesity. *J Nutr*. 1982;112:2314–2323.

20. Etherton TD, Kris-Etherton PM. Characterization of plasma lipoproteins in swine with different propensities for obesity. *Lipids*. 1980;15:823–829.

21. Neeb ZP, Edwards JM, Alloosh M, Long X, Mokelke EA, Sturek M. Metabolic syndrome and coronary artery disease in Ossabaw compared with Yucatan swine. *Comp Med*. 2010;60:300–315.

22. Bell LN, Lee L, Saxena R, Bemis KG, Wang M, Theodorakis JL, Vuppalanchi R, Alloosh M, Sturek M, Chalasani N. Serum proteomic analysis of diet-induced steatohepatitis and metabolic syndrome in the Ossabaw miniature swine. *Am J Physiol Gastrointest Liver Physiol*. 2010;298:G746–G754.

23. Lassaletta AD, Chu LM, Robich MP, Elmadhun NY, Feng J, Burgess TA, Laham RJ, Sturek M, Sellke FW. Overfed Ossabaw swine with early stage metabolic syndrome have normal coronary collateral development in response to chronic ischemia. *Basic Res Cardiol*. 2012;107:243.

24. Lee L, Alloosh M, Saxena R, Van Alstine W, Watkins BA, Klaunig JE, Sturek M, Chalasani N. Nutritional model of steatohepatitis and metabolic syndrome in the Ossabaw miniature swine. *Hepatology*. 2009;50:56–67.

25. Newell-Fugate AE. Validation of the obese Ossabaw miniature pig as a model of the obese polycystic ovary syndrome phenotype with concomitant metabolic syndrome: exploration of polycystic ovary syndrome pathophysiology using in vivo and in vitro models. *Anim Sci*. Availlable at: https://www.ideals.illinois.edu/bitstream/handle/2142/42187/Anne_Newell-Fugate.pdf?sequence=1. Accessed March 13, 2018.

26. Newell-Fugate AE, Taibl JN, Clark SG, Alloosh M, Sturek M, Krisher RL. Effects of diet-induced obesity on metabolic parameters and reproductive function in female Ossabaw minipigs. *Comp Med*. 2014;64:44–49.

27. Potu RB, Lu H, Adeola O, Ajuwon KM. Metabolic markers in Ossabaw pigs fed high fat diets enriched in regular or low alpha-linolenic acid soy oil. *Nutr Metab (Lond)*. 2013;10:27.

28. Wastney M, Lee W, Jackson GS, Alloosh M, Sturek M, Lachcik P, Peacock M, Martin B, Weaver CM. Soft tissue calcification in the Ossabaw miniature pig: experimental and kinetic modeling studies. *Osteoporos Int*. 2013;24:2123–2126.

29. Clark KJ, Carlson DF, Foster LK, Kong BW, Foster DN, Fahrenkrug SC. Enzymatic engineering of the porcine genome with transposons and recombinases. *BMC Biotechnol*. 2007;7:42.

30. Carlson DF, Garbe JR, Tan W, Martin MJ, Dobrinsky JR, Hackett PB, Clark KJ, Fahrenkrug SC. Strategies for selection marker-free swine transgenesis using the sleeping beauty transposon system. *Transgenic Res*. 2011;20:1125–1137.

31. Collas P. Dedifferentiation of cells: new approaches. *Cytotherapy*. 2007;9:236–244.

32. Langmead B, Salzberg SL. Fast gapped-read alignment with bowtie 2. *Nat Methods*. 2012;9:357–359.

33. Li H, Handsaker B, Wysoker A, Fennell T, Ruan J, Homer N, Marth G, Abecasis G, Durbin R; 1000 Genome Project Data Processing Subgroup. The sequence alignment/map format and samtools. *Bioinformatics*. 2009;25:2078–2079.

34. Lee WP, Stromberg MP, Ward A, Stewart C, Garrison EP, Marth GT. MOSAIK: a hash-based algorithm for accurate next-generation sequencing short-read mapping. *PLoS One*. 2014;9:e90581.

35. Guensch DP, Fischer K, Flewitt JA, Friedrich MG. Impact of intermittent apnea on myocardial tissue oxygenation: a study using oxygenation-sensitive cardiovascular magnetic resonance. *PLoS One*. 2013;8:e53282.

36. Kara B, Nayman A, Guler I, Gul EE, Koplay M, Paksoy Y. Quantitative assessment of left ventricular function and myocardial mass: a comparison of coronary CT angiography with cardiac MRI and echocardiography. *Pol J Radiol*. 2016;81:95–102.

37. Brown AJ, Obaid DR, Costopoulos C, Parker RA, Calvert PA, Teng Z, Hoole SP, West NE, Goddard M, Bennett MR. Direct comparison of virtual-histology intravascular ultrasound and optical coherence tomography imaging for identification of thin-cap fibroatheroma. *Circ Cardiovasc Imaging*. 2015;8:e003487.

38. Pawar AS, Zhu XY, Eirin A, Tang H, Jordan KL, Woollard JR, Lerman A, Lerman LO. Adipose tissue remodeling in a novel domestic porcine model of diet-induced obesity. *Obesity (Silver Spring)*. 2015;23:399–407.

39. Zhang X, Li ZL, Eirin A, Ebrahimi B, Pawar AS, Zhu XY, Lerman A, Lerman LO. Cardiac metabolic alterations in hypertensive obese pigs. *Hypertension*. 2015;66:430–436.

40. Li ZL, Ebrahimi B, Zhang X, Eirin A, Woollard JR, Tang H, Lerman A, Wang SM, Lerman LO. Obesity-metabolic derangement exacerbates cardiomyocyte

loss distal to moderate coronary artery stenosis in pigs without affecting global cardiac function. *Am J Physiol Heart Circ Physiol*. 2014;306:H1087–H1101.

41. Dey D, Wong ND, Tamarappoo B, Nakazato R, Gransar H, Cheng VY, Ramesh A, Kakadiaris I, Germano G, Slomka PJ, Berman DS. Computer-aided non-contrast CT-based quantification of pericardial and thoracic fat and their associations with coronary calcium and metabolic syndrome. *Atherosclerosis*. 2010;209:136–141.

42. Boogers MJ, Schuijf JD, Kitslaar PH, van Werkhoven JM, de Graaf FR, Boersma E, van Velzen JE, Dijkstra J, Adame IM, Kroft LJ, de Roos A, Schreur JH, Heijenbrok MW, Jukema JW, Reiber JH, Bax JJ. Automated quantification of stenosis severity on 64-slice CT: a comparison with quantitative coronary angiography. *JACC Cardiovasc Imaging*. 2010;3:699–709.

43. Arbab-Zadeh A, Hoe J. Quantification of coronary arterial stenoses by multidetector CT angiography in comparison with conventional angiography methods, caveats, and implications. *JACC Cardiovasc Imaging*. 2011;4:191–202.

44. Malago R, D'Onofrio M, Tavella D, Mantovani W, Brunelli S, Pezzato A, Caliari G, Nicoli L, Benussi P, Mucelli RP. Diagnostic accuracy in coronary stenosis: comparison between visual score and quantitative analysis (quantitative computed tomographic angiography) in coronary angiography by multidetector computed tomography-coronary angiography and quantitative analysis (quantitative coronary angiography) in conventional coronary angiography. *J Comput Assist Tomogr*. 2010;34:652–659.

45. Moritz R, Eaker DR, Anderson JL, Kline TL, Jorgensen SM, Lerman A, Ritman EL. IVUS detection of vasa vasorum blood flow distribution in coronary artery vessel wall. *JACC Cardiovasc Imaging*. 2012;5:935–940.

46. Park KH, Kwon TG, Matsuzawa Y, Sun T, Liu Z, Lennon RJ, Lerman LO, Kushwaha SS, Lerman A. Association between the vasa vasorum and the atherosclerotic changes in cardiac allograft vasculopathy: volumetric analysis. *Eur Heart J Cardiovasc Imaging*. 2016;17:272–279.

47. Aoki T, Rodriguez-Porcel M, Matsuo Y, Cassar A, Kwon TG, Franchi F, Gulati R, Kushwaha SS, Lennon RJ, Lerman LO, Ritman EL, Lerman A. Evaluation of coronary adventitial vasa vasorum using 3D optical coherence tomography: animal and human studies. *Atherosclerosis*. 2015;239:203–208.

48. Tearney GJ, Regar E, Akasaka T, Adriaenssens T, Barlis P, Bezerra HG, Bouma B, Bruining N, Cho JM, Chowdhary S, Costa MA, de Silva R, Dijkstra J, Di Mario C, Dudek D, Falk E, Feldman MD, Fitzgerald P, Garcia-Garcia HM, Gonzalo N, Granada JF, Guagliumi G, Holm NR, Honda Y, Ikeno F, Kawasaki M, Kochman J, Koltowski L, Kubo T, Kume T, Kyono H, Lam CC, Lamouche G, Lee DP, Leon MB, Maehara A, Manfrini O, Mintz GS, Mizuno K, Morel MA, Nadkarni S, Okura H, Otake H, Pietrasik A, Prati F, Raber L, Radu MD, Rieber J, Riga M, Rollins A, Rosenberg M, Sirbu V, Serruys PW, Shimada K, Shinke T, Shite J, Siegel E, Sonoda S, Suter M, Takarada S, Tanaka A, Terashima M, Thim T, Uemura S, Ughi GJ, van Beusekom HM, van der Steen AF, van Es GA, van Soest G, Virmani R, Waxman S, Weissman NJ, Weisz G. Consensus standards for acquisition, measurement, and reporting of intravascular optical coherence tomography studies: a report from the international working group for intravascular optical coherence tomography standardization and validation. *J Am Coll Cardiol*. 2012;59:1058–1072.

49. Eirin A, Williams BJ, Ebrahimi B, Zhang X, Crane JA, Lerman A, Textor SC, Lerman LO. Mitochondrial targeted peptides attenuate residual myocardial damage after reversal of experimental renovascular hypertension. *J Hypertens*. 2014;32:154–165.

50. Virmani R, Kolodgie FD, Burke AP, Farb A, Schwartz SM. Lessons from sudden coronary death: a comprehensive morphological classification scheme for atherosclerotic lesions. *Arterioscler Thromb Vasc Biol*. 2000;20:1262–1275.

51. Kreutz RP, Alloosh M, Mansour K, Neeb Z, Kreutz Y, Flockhart DA, Sturek M. Morbid obesity and metabolic syndrome in Ossabaw miniature swine are associated with increased platelet reactivity. *Diabetes Metab Syndr Obes*. 2011;4:99–105.

52. Miller M, Stone NJ, Ballantyne C, Bittner V, Criqui MH, Ginsberg HN, Goldberg AC, Howard WJ, Jacobson MS, Kris-Etherton PM, Lennie TA, Levi M, Mazzone T, Pennathur S; American Heart Association Clinical Lipidology, Thrombosis, and Prevention Committee of the Council on Nutrition, Physical Activity, and Metabolism; Council on Arteriosclerosis, Thrombosis, and Vascular Biology; Council on Cardiovascular Nursing; Council on the Kidney in Cardiovascular Disease. Triglycerides and cardiovascular disease: a scientific statement from the American Heart Association. *Circulation*. 2011;123:2292–2333.

53. Meserole VK, Etherton TD. Insulin binding to liver microsomes from lean and obese swine during growth to market weight. *J Anim Sci*. 1984;59:650–657.

54. Wangsness PJ, Martin RJ, Gahagan JH. Insulin and growth hormone in lean and obese pigs. *Am J Physiol*. 1977;233:E104–E108.

55. Al-Mashhadi RH, Bjorklund MM, Mortensen MB, Christoffersen C, Larsen T, Falk E, Bentzon JF. Diabetes with poor glycaemic control does not promote atherosclerosis in genetically modified hypercholesterolaemic minipigs. *Diabetologia*. 2015;58:1926–1936.

56. Tuzcu EM, Bayturan O, Kapadia S. Invasive imaging: coronary intravascular ultrasound: a closer view. *Heart*. 2010;96:1318–1324.

57. Zhu XY, Daghini E, Chade AR, Versari D, Krier JD, Textor KB, Lerman A, Lerman LO. Myocardial microvascular function during acute coronary artery stenosis: effect of hypertension and hypercholesterolaemia. *Cardiovasc Res*. 2009;83:371–380.

58. Rodriguez-Porcel M, Lerman A, Ritman EL, Wilson SH, Best PJ, Lerman LO. Altered myocardial microvascular 3D architecture in experimental hypercholesterolemia. *Circulation*. 2000;102:2028–2030.

59. Elezaby A, Sverdlov AL, Tu VH, Soni K, Luptak I, Qin F, Liesa M, Shirihai OS, Rimer J, Schaffer JE, Colucci WS, Miller EJ. Mitochondrial remodeling in mice with cardiomyocyte-specific lipid overload. *J Mol Cell Cardiol*. 2015;79:275–283.

60. Zhu XY, Rodriguez-Porcel M, Bentley MD, Chade AR, Sica V, Napoli C, Caplice N, Ritman EL, Lerman A, Lerman LO. Antioxidant intervention attenuates myocardial neovascularization in hypercholesterolemia. *Circulation*. 2004;109:2109–2115.

61. Yan RT, Miller JM, Rochitte CE, Dewey M, Niinuma H, Clouse ME, Vavere AL, Brinker J, Lima JA, Arbab-Zadeh A. Predictors of inaccurate coronary arterial stenosis assessment by CT angiography. *JACC Cardiovasc Imaging*. 2013;6:963–972.

62. Ding K, McDonough SJ, Kullo IJ. Evidence for positive selection in the C-terminal domain of the cholesterol metabolism gene PCSK9 based on phylogenetic analysis in 14 primate species. *PLoS One*. 2007;2:e1098.

63. Frank-Kamenetsky M, Grefhorst A, Anderson NN, Racie TS, Bramlage B, Akinc A, Butler D, Charisse K, Dorkin R, Fan Y, Gamba-Vitalo C, Hadwiger P, Jayaraman M, John M, Jayaprakash KN, Maier M, Nechev L, Rajeev KG, Read T, Rohl I, Soutschek J, Tan P, Wong J, Wang G, Zimmermann T, de Fougerolles A, Vornlocher HP, Langer R, Anderson DG, Manoharan M, Koteliansky V, Horton JD, Fitzgerald K. Therapeutic RNAi targeting PCSK9 acutely lowers plasma cholesterol in rodents and LDL cholesterol in nonhuman primates. *Proc Natl Acad Sci U S A*. 2008;105:11915–11920.

64. Bellinger DA, Merricks EP, Nichols TC. Swine models of type 2 diabetes mellitus: insulin resistance, glucose tolerance, and cardiovascular complications. *ILAR J*. 2006;47:243–258.

65. Hamamdzic D, Wilensky RL. Porcine models of accelerated coronary atherosclerosis: role of diabetes mellitus and hypercholesterolemia. *J Diabetes Res*. 2013;2013:761415.

66. Litten-Brown JC, Corson AM, Clarke L. Porcine models for the metabolic syndrome, digestive and bone disorders: a general overview. *Animal*. 2010;4:899–920.

67. Spurlock ME, Gabler NK. The development of porcine models of obesity and the metabolic syndrome. *J Nutr*. 2008;138:397–402.

SUPPLEMENTAL MATERIAL

Table S1. Comparison of Founder Swine Blood Lipoproteins by Nuclear Magnetic Resonance.

	Particle Concentration (Mean Particle Size in nm)		
	HDL (µmol/l)	VLDL (nmol/l)	LDL (nmol/l)
Control *(N=2)*	25.9 ± 8.6 (8.7 ± 0.07)	8.75 ± 1.5 (58.7 ± 5.23)	541 ± 31 (19.9 ± 0.8)
Landrace *PCSK9* GOF *(N=2)*	10.5 ± 4 (10.25 ± 0.35)	128 ± 52 (33.05 ± 0.07)	1821 ± 409 (20.9 ± 0.14)
Ossabaw *PCSK9* GOF *(N=1)*	16.2 (9.8)	139 (32.9)	2280 (20.6)

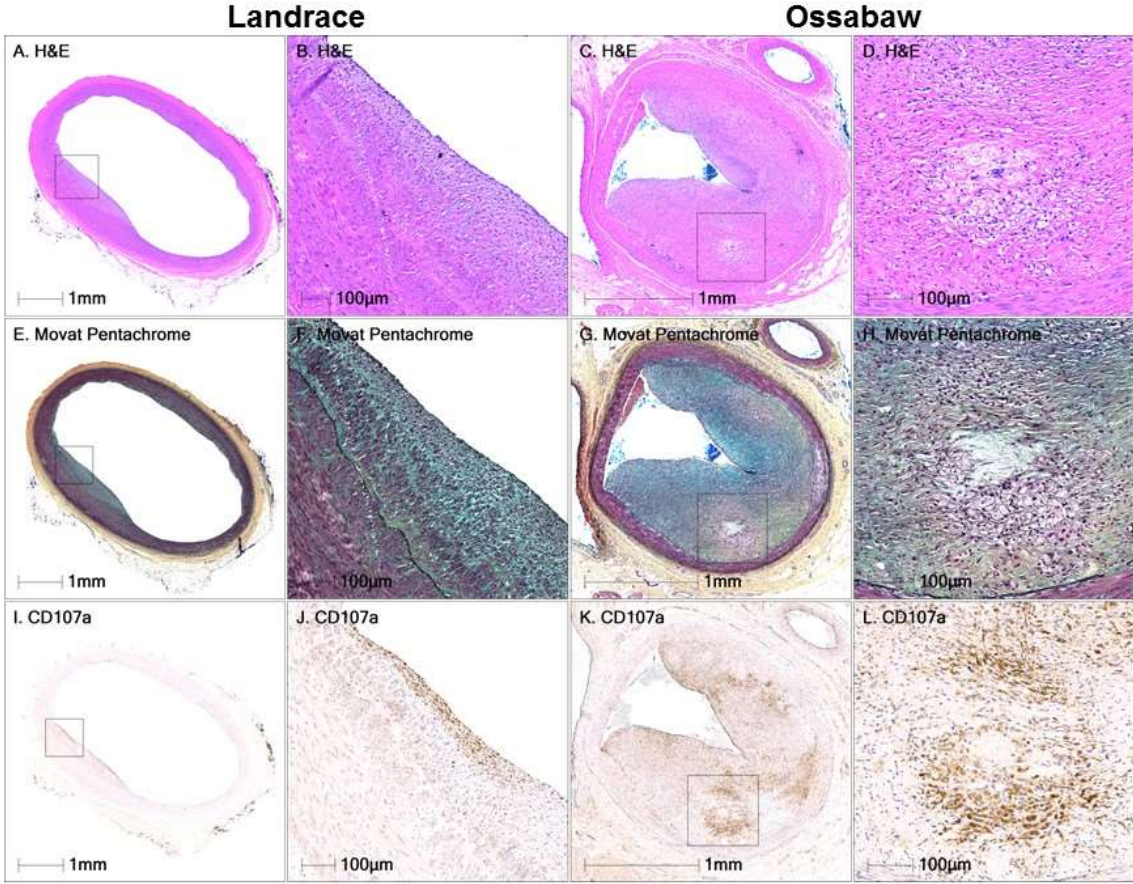No statistics were done due to low number of founder animals for comparison

Table S2. Comparison of Cardiac Function.

Group	Control		PCSK9 GOF		PCSK9 GOF ATH Diet	
Age	6 months	9 months	6 months	9 months	6 months	9 months
Heart Rate^{SED} Heart Rate^{AMB} (beats/min)	70.7 ± 21.5 67.0 ± 14.9	60.7 ± 17.5 64.4 ± 14.3	73.6 ± 13.9 71.3 ± 10.6	65.9 ± 6.5 58.9 ± 5.0	75.6 ± 9.0 69.7 ± 16.0	82.3 ± 13.4‡† 61.0 ± 10.4
Mean Arterial Pressure* (mmHg)	117.6 ± 13.5	118.4 ± 18.7	120.6 ± 9.3	120.6 ± 9.7	113.9 ± 13.1	117.4 ± 7.5
EDV	81.2 ± 5.4	87.1 ± 11.3	66.6 ± 9.8‡	81.0 ± 15.6†	63.8 ± 5.0‡	73.9 ± 7.2†
ESV	34.2 ± 3.5	42.0 ± 11.2	25.8 ± 4.8‡	24.8 ± 4.8‡	25.8 ± 2.9‡	27.6 ± 4.0‡
LVM (g)	67.2 ± 7.6	68.3 ± 6.4	60.1 ± 4.5	77.7 ± 9.6$^{†‖}$	57.2 ± 3.7‡†	66.7 ± 4.0†
Ejection Fraction (%)	57.7 ± 3.1	52.1 ± 11.3	61.3 ± 3.2	69.2 ± 2.8†‡	59.6 ± 3.4	62.7 ± 3.9
Cardiac Output (l/min)	3.3 ± 1.0	2.7 ± 0.8	3.0 ± 0.7	3.7 ± 0.9	2.9 ± 0.3	3.8 ± 0.7†
Myocardial Perfusion (ml/min/g)	1.1 ± 0.2	1.0 ± 0.4	1.3 ± 0.4	1.2 ± 0.2	1.4 ± 0.4	1.4 ± 0.3
Pericardial Fat (%)	0.06 ± 0.01	0.07 ± 0.02	0.05 ± 0.01	0.06 ± 0.01	0.06 ± 0.01	0.07 ± 0.01
Glucose (mg/dL)	116 ± 7.6	135 ± 41.1	139 ± 52.5	159 ± 27.0	163 ± 48.6‡	141 ± 17.6
Insulin (mmol/L)	0.23 ± 0.13	0.38 ± 0.22	0.20 ± 0.1	0.18 ± 0.09‡	0.36 ± 0.25	0.21 ± 0.08‡

Mean ± SD shown for each. Mean arterial pressure was recorded in ambulatory animals. † $p < 0.05$ vs. same group at 6 months of age; ‡ $p < 0.05$ vs. control at same age; § $p < 0.05$ vs. all other groups; ‖ $p < 0.05$ vs. PCSK9 GOF ATH Diet at same age. Variance of means between study groups were analyzed by one way ANOVA, and where significant, all pairs comparison of means using Tukey-Kramer HSD method. Mean difference within groups determined by matched pairs repeated measures analysis followed by two-tailed t-testing.
LVM: left ventricular mass; ESV: End systolic volume; EDV: End diastolic volumes; AMB: ambulatory; SED: sedated.

Figure S1. Ectopic *Pt*PCSK9^{D374Y} expression reduces hepatic expression of LDLR.

A, Serum PCSK9 levels, *p<0.05 compared to Control using ANOVA followed by t-tests. **B,**

Western blot shows decreased LDLR detection in liver extracts in GOF groups.

Figure S2. Representative Lesions from LCX Artery of PCSK9 GOF Founders.

A-L, Left circumflex artery (LCX); Landrace founder at 14 months of age; Ossabaw founder at 15 months of age; Histologic coronary staining: hematoxylin & eosin (H&E) (**A-D**), modified Movat's Pentachrome (**E-H**), Immunohistochemistry staining for CD107a highlighting inflammation (**I-L**).

Figure S3. Myocardial fibrosis in PCKS9 GOF animals.
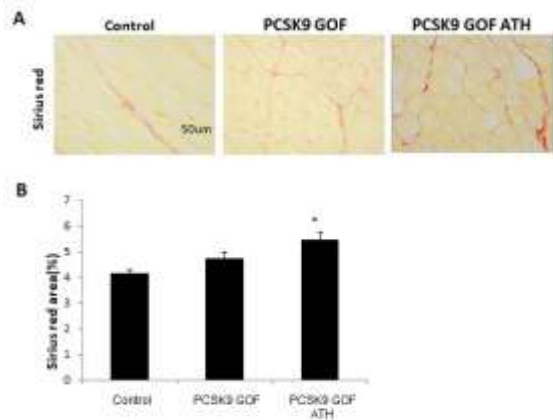
A, Representative Sirius Red stating in left ventricle myocardial tissue. **B,** Quantification of Sirius Red staining in each group was analyzed using ANOVA followed by t-tests. *p<0.05 compared to Control.

Figure S4. Coronary artery lesion measurements by quantitative coronary angiography (CT images) in Ossabaw pigs at 9 months of age.
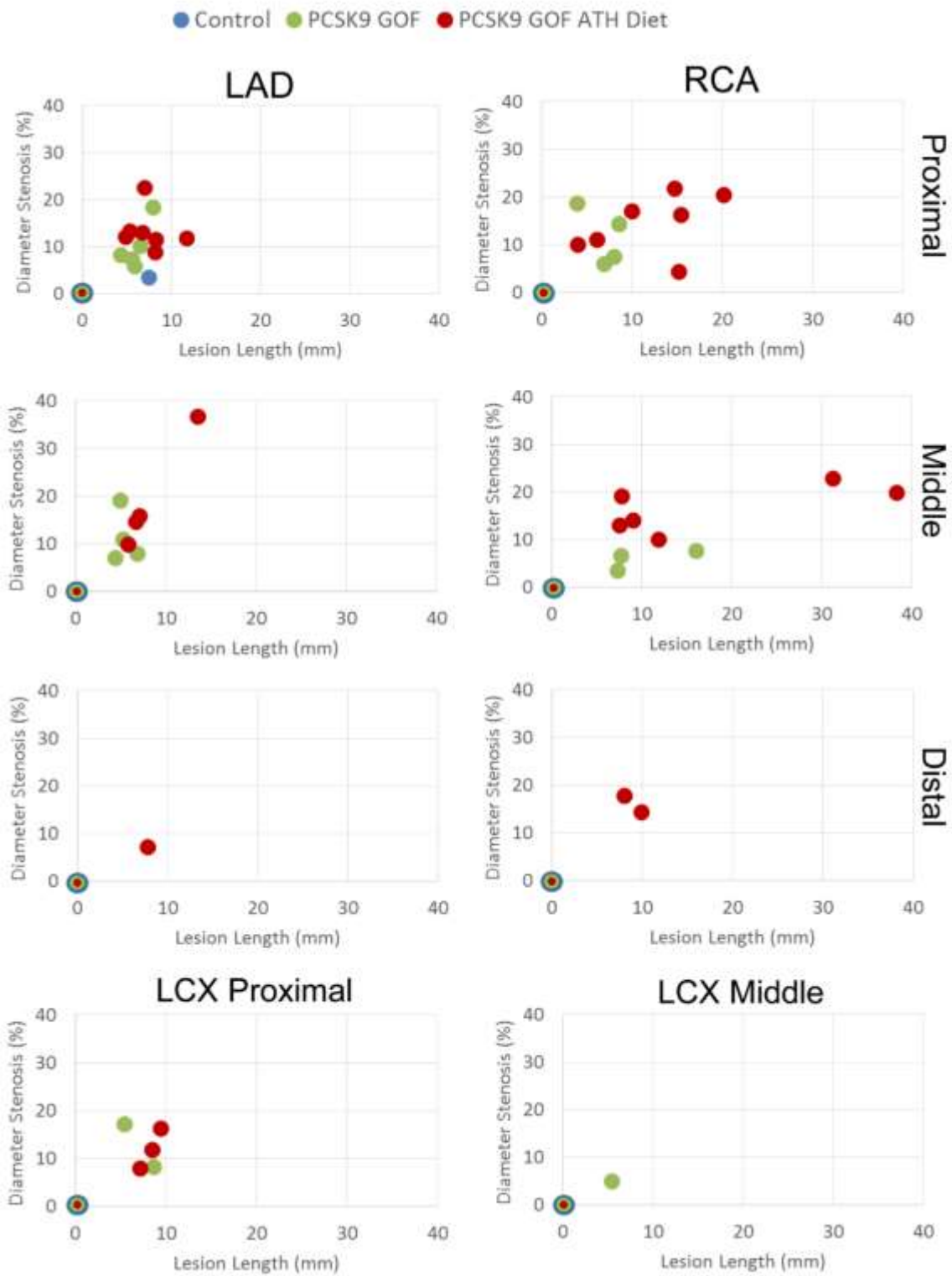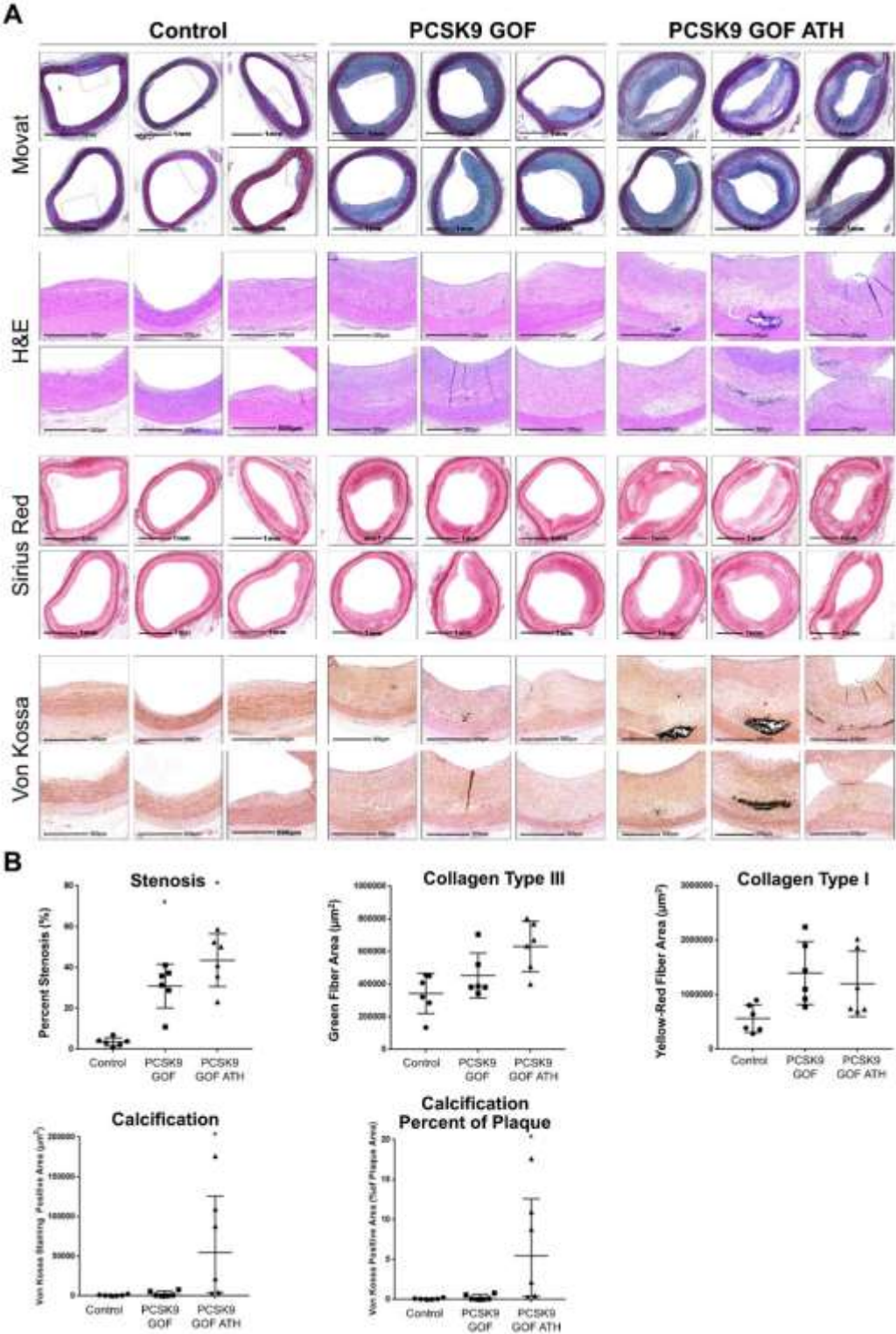
Figure S5. Histopathological features of plaques in the LAD.

A, Representative histopathological features of the most stenotic section of the proximal left anterior descending (LAD) from different individual animals at 9 months of age. The higher power magnifications (H&E and von Kossa stains) represent regions corresponding to the red box in the low power Movat's Pentachrome stain. Histologic coronary staining top to bottom: modified Movat's Pentachrome; hematoxylin & eosin (H&E), picrosirius red; and von Kossa (highlighting calcium). Scale Bar: low power image=1mm; higher power=500µm. **B**, Sirius Red staining images taken on BX51 Olympus microscope under polarized light were used for collagen quantification; the percentage of stenosis were also quantified in the displayed images. Values displayed are means and standard deviations. Calcification area in plaque and percent of plaque area was quantified from the displayed von Kossa stained images with median ± interquartile values displayed.   *p<0.05 compared to Control; † p<0.05 compared to PCSK9 GOF on standard diet using one-way ANOVA, multiple comparison analysis. Calcification data was analyzed by Kruskal-Wallis testing followed by Dunn's multiple comparison.

Figure S6. Immunohistochemical analysis of plaques in the LAD.
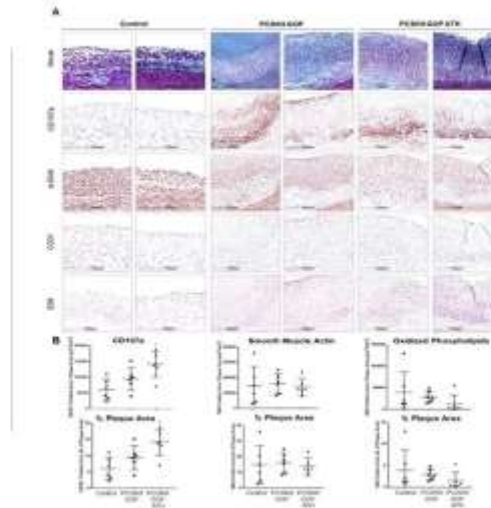
A, Immunohistochemistry staining for CD107a, smooth muscle actin (SMA), CD31, and E06 highlights inflammation, neointimal hyperplasia, endothelial cells, and oxidized phospholipids respectively, predominantly in GOF groups. **B**, CD107a, SMA immunostaining areas were quantified on HALO platform (Indica Labs, Corrales, NM), and results were presented as total CD107a or SMA positive area and the percentage of plaque area. Mean and standard deviation is displayed. Analysis was performed using one way ANOVA, multiple comparison analysis. *p<0.05 compared to Control; † p<0.05 compared to PCSK9 GOF on standard diet.